A Critical Review of Charged Particle Astronomy at Saturn: The Evidence for Co-orbiting Material in the Inner Satellite System

NASA-Ames Grant No. 2-528

FINAL TECHNICAL REPORT

(7/01/88 - 11/30/89)

by

John P. Wefel
Principal Investigator
Professor of Physics

John F. Cooper
Co-Investigator
Senior Research Associate

Department of Physics and Astronomy
Louisiana State University
Baton Rouge, LA 70803

submitted to

Dr. J. N. Cuzzi, Technical Officer
University Affairs Branch, 241-25
NASA Ames Research Center
Moffett Field, CA 94035

October 15, 1990

A Critical Review of Charged Particle Astronomy at Saturn:

The Evidence for Co-orbiting Material in the Inner Satellite System

SUMMARY

Agreement NAG 2-528 was designed to support Dr. John F. Cooper's work on reassessment of the charged particle observations from Pioneer and Voyager at Saturn with a view towards providing limits on the amount of "unseen" dust and debris that may exist in the Saturnian system. Such estimates are crucial for planning the Cassini tour of Saturn. The data from Pioneer-11 and Voyager were reviewed, intercompared and correlated with model predictions to set limits on the matter distribution. The results were presented at several meetings and incorporated into the Cassini Proposal Information Package.

BIBLIOGRAPHY

"Review of Pioneer 11 Data for High Energy Trapped Radiation in Saturn's Magnetosphere," W. Fillius, J. F. Cooper, and R. B. McKibben, *Trans. Am. Geophys. Union (EOS), 69*, 1398 (1988).

"Abundance and Size Distribution of Ring Material Outside the Main Rings of Saturn," J. N. Cuzzi, J. F. Cooper, L. L. Hood, and M. R. Showalter, in *Cassini Mission: Saturn Orbiter Proposal Information Package, JPL PD 699-11, Vol. XIII: Physical Models,* p. 5-1 (1989).

"A Critical Review of Charged Particle Astronomy at Saturn: The Evidence for Co-orbiting Material in the Inner Satellite System," J. F. Cooper, in *Cassini Mission: Saturn Orbiter Proposal Information Package, JPL PD 699-11, Vol. XIII: Physical Models,* p. 5-C-1 (1989).

"Interaction of Matter and Energetic Radiation in the Inner Saturn System," J. F. Cooper, presented to IAGA 1989 Assembly, Planetary Magnetospheres Symposium, Exeter, England (July, 1989).

"Energetic Particle Interactions with Planetary Material in the Saturn System," J. F. Cooper and J. P. Wefel, Proc. 21st Int. Cosmic Ray Conf., Adelaide, 7, 260, (1990).

"Applications of Energetic Particle Spectroscopy to the Investigation of Ring and Satellite Systems in the Outer Planet Magnetospheres," J. F. Cooper, *Conference Abstracts, Fred Scarf Memorial Symposium on Magnetospheres of the Outer Planets,* Annapolis, MD, (August, 1990).

"Satellite Sweeping of Electrons at Neptune and Uranus," J. F. Cooper, Geophys. Res. Letters, 17, 1665 (1990).

TECHNICAL DISCUSSION

prepared by: John F. Cooper

Department of Physics and Astronomy
Louisiana State University
Baton Rouge, Louisiana 70803

1. Introduction

The planetary system and magnetosphere of Saturn has been studied *in-situ* by three flyby missions: Pioneer 11 in 1979 [Opp, 1980], Voyager 1 in 1980 [Stone and Miner, 1981], and Voyager 2 in 1981 [Stone and Miner, 1982]. All three spacecraft were fully instrumented for measurements of energetic charged particles, but only Pioneer 11 covered the full range of the magnetosphere into the inner planetary system as shown in Figure 1. The first measurements of high energy trapped radiation were reported by the Pioneer 11 investigators [Fillius *et al.*, 1980; Fillius and McIlwain, 1980; Simpson *et al.*, 1980a,b, 1981; Van Allen *et al.*, 1980a,b] and further measurements with higher resolution in energy and direction were made by Voyager 2 [Krimigis *et al.*, 1982, 1983; Krimigis and Armstrong, 1982; McDonald *et al.*, 1980; Schardt and McDonald, 1983; Trainor *et al.*, 1980; Vogt *et al.*, 1982] The nearly equatorial flyby trajectory of Pioneer 11 was especially well-suited for measurements of radial distributions and time dependence (i.e., inbound versus outbound) of stably trapped particles, while the Voyager 2 trajectory covered a larger range of magnetic latitudes at $L \geq 2.73$ and was more useful for measurements of pitch angle distributions [e.g., Schardt and McDonald, 1983; Schardt, 1983].

Ongoing plans [Stetson, 1989; Nicholson, 1989] for the next mission to Saturn, Cassini, call for an four-year tour of the Saturn system by the Cassini orbiter spacecraft after release of the Titan probe. If properly instrumented, the orbiter tour will allow very detailed surveys of trapped particles within the magnetosphere and over the main rings. While providing valuable new scientific information on the magnetospheric trapped radiation and its interaction with rings, satellites, other co-orbiting bodies, and dust in the Saturn system, charged particle measurements may also provide a critical capability for assessing probable abundances, or upper limits thereof, for material posing potentially significant impact hazards. Since the tour will require many crossings of the equatorial ring plane within and inwards of the E-ring region, there is a clear need to evaluate the relative merits of different radial positions for these crossings, so that that impact hazards may be minimized.

The present review specifically addresses the most relevant observations of energetic trapped particles from Pioneer and Voyager for the indirect survey of co-orbiting material via trapped particle absorption. While absorption effects of the major rings and satellites are clearly evident in the observations, the most critical questions for Cassini concern limits that may be placed on abundances of diffuse dust and larger debris which are not well-constrained by other observations. Although Voyager and/or earth-based observations have measured the total optical opacities of the G- and E-rings, these opacities are dominated by contributions from small, micron-sized dust particles when measured with backscattered sunlight. Particles above a few hundred microns in size pose the greatest impact hazards,

make little contribution to optical opacity, and may be better assessed by absorption of trapped radiation.

The most useful trapped particle observations for the present review fall in three categories: (1) high energy protons, which have very long trapping times (i.e., years) and correspondingly high probabilities for interaction with low-opacity dust material (if present), (2) high intensity electrons at energies near a few MeV, which show significant response to magnetospheric perturbations on hour time scales and can only be used for sampling of high-opacity absorbers, and (3) higher energy electrons which may arise in part as secondary products of proton-dust interactions. The principal focii of discussion are (1), which has a reasonably well-known source rate from cosmic ray albedo neutron decay (CRAND), and the potential evidence for the existence of (3), which might provide the best constraints on dust abundances if measured by appropriate instruments on the Cassini orbiter. We will also discuss "microsignature" observations which may indicate the presence of large abundances of localized (but unseen) dust clouds co-orbiting with the principal satellites, although uncertainties (viz-a-viz electron background) remain in interpretation of the charged particle data for some microsignatures. All of the above categories are recommended for measurements by orbiter instrumentation during the early phases of the Cassini mission.

Despite the indirect nature of the charged particle measurements for detection of absorbing dust and/or larger bodies, such measurements offer an important advantage over direct, *in-situ* measurements with dust detectors. The charged particle surveys can be carried out rapidly during the first few passes of the orbiter through the inner magnetosphere over a wide radial range in relative safety away from the equatorial region. In contrast the *in-situ* measurements can only be made at selected equatorial crossings where one has already estimated that the dust densities will be minimal. A complementary arrangement would be that the charged particle data be used for the initial wide-ranging surveys, while later *in-situ* observations would be planned for ring-plane crossings at specific points of interest. Regions of high trapped proton intensities can be chosen for the initial aim points at the ring plane before and after SOI to minimize risks during the first surveys. On the other hand there may be a an understandable desire by mission planners to avoid *any* regions of interest for direct dust measurements that appear even marginally hazardous from the charged particle survey. Thus the charged particle data may have the more crucial role for hazard assessment.

High resolution science data on species, energy spectra, and directionality of high energy trapped radiation would allow prolonged study of sources, radial transport, and sinks while also providing critical remote-sensing information for assessment of spacecraft hazards associated with selection of sites for ring plane crossings during the four-year mission. Although high energy measurements of trapped radiation have been made for many years in the terrestrial magnetosphere, Saturn offers a unique new environment to study interactions of this radiation with the planetary environment, such that significant new contributions may be made to magnetospheric and planetary science. By the time the Cassin orbiter finishes its presently conceived mission at Saturn by about the year 2010, the earth's man-made "rings" wil be dense enough to significantly absorb CRAND protons in the earth's magnetosphere [Konradi, 1988], so that the study of dust-magnetosphere interactions may become increasingly important for assessing hazards from debris impacts with respect to unmanned and manned space operations near Earth as well as at Saturn.

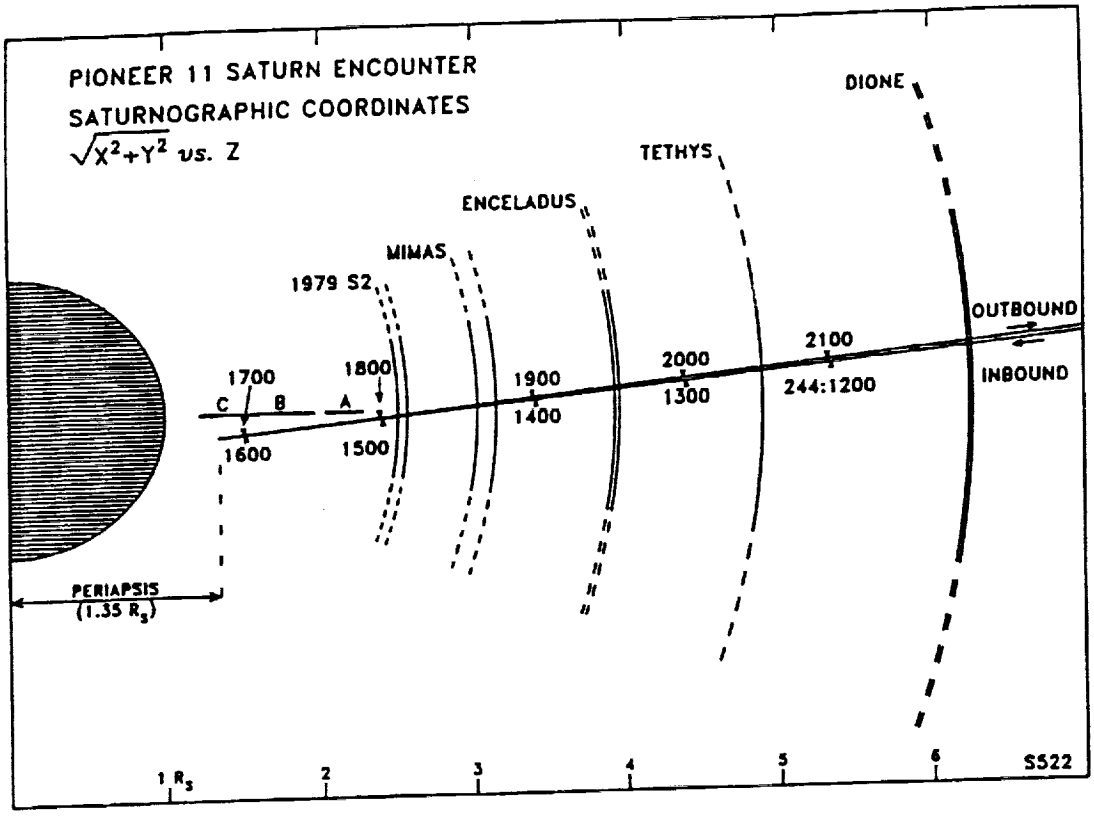

Figure 1: Pioneer 11 trajectory in the inner Saturn system [Simpson *et al.*, 1980b].

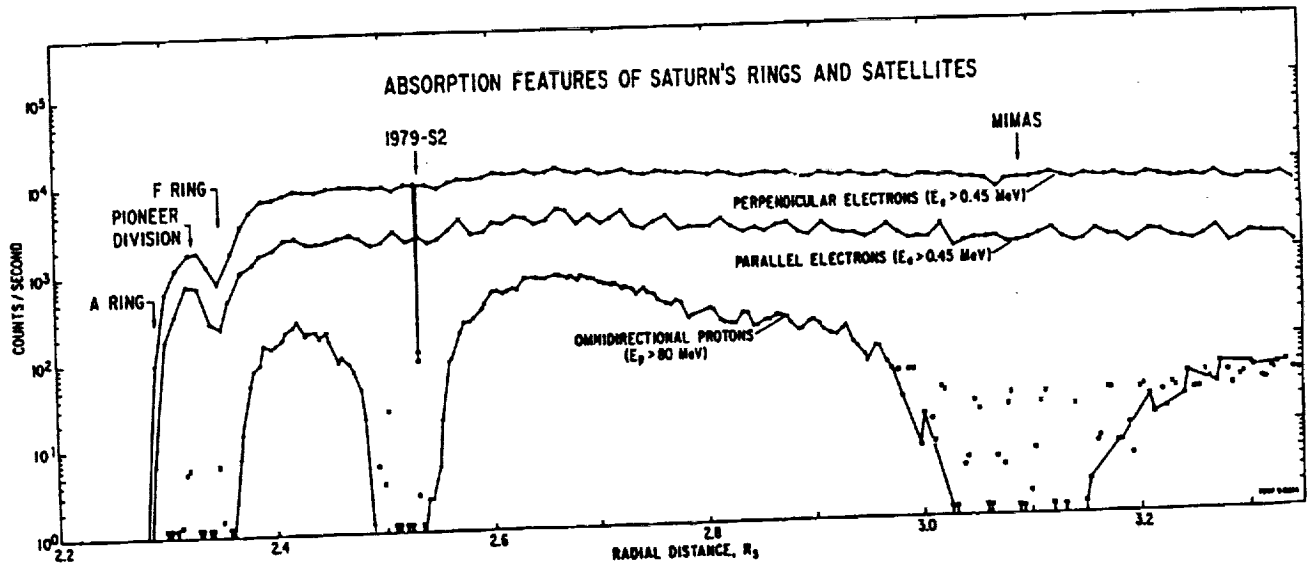

Figure 2: Inbound counting rate profiles in Saturn's inner magnetosphere from Pioneer 11 for electrons > 0.45 MeV and protons > 80 MeV [Fillius *et al.*, 1980]. Directional components are shown for electrons with velocities perpendicular and parallel to the local magnetic field direction. The proton rates are averaged over all directions of incidence. The feature labeled "1979-S2" is a microsignature in the orbital region of Janus and Epimetheus.

2. Observations of Energetic Trapped Radiation

Sources

High energy trapped protons and electrons in the inner magnetosphere of Saturn have complex interactions with planetary rings, satellites, and dust in the Saturn System. Nuclear interactions of very high energy ($\geq$ 20 GeV/N) cosmic ray protons and nuclei with Saturn's main rings produce secondary particles at sub-GeV energies with high efficiency [Blake *et al.*, 1983; Cooper, 1983; Cooper *et al.*, 1985]. The charged secondaries have low level intensities within the ring region due to rapid reabsorption by the ring material, while the neutral secondary components (neutrons and gamma rays) can radiate away from the rings. Beta decay of the secondary neutrons (CRAND) provides the only known source of protons above 10 MeV in the trapped radiation belts of the inner magnetosphere.

The beta-decay protons are trapped with essentially all of the parent neutron energy and can undergo further interactions with satellites and more diffuse material orbiting around Saturn near the equatorial ring plane. A significant fraction of the trapped protons are sufficiently energetic to produce pions from interaction with dust grains, thereby populating the radiation belts with highly relativistic (10-100 MeV) electrons from pion-muon decays. Inward radial diffusion and betatron acceleration of sub-MeV electrons from the outer magnetosphere provides a much higher intensity population of electrons at energies below five MeV. The relative intensities of these trapped secondary interaction products are in turn controlled by lifetimes for radial transport within the inner magnetosphere and re-absorption by satellites and diffuse material.

Radial Profiles

The Pioneer 11 data of Fillius *et al.* (1980) are shown in Figures 2 and 3 to illustrate the entirely different radial profiles of the trapped electron and CRAND proton components in the inner magnetosphere. Despite the very low injection rates from CRAND, the fluxes of high energy protons build up to high levels in radial zones not swept by the main rings, the F-ring, the co-orbiting satellites Epimetheus and Janus, and the innermost principal moons, Mimas and Enceladus. Since the rate of source injection varies slowly across the proton trapping regions, the relative magnitudes of proton intensities in these regions are primarily due to diffusive effects [see Section 3]. There is no obvious effect of absorption by diffuse dust other than the inflection in the proton profile in the vicinity of the G ring near 2.8 R_S, although dust losses might be masked by radial variations arising from diffusion.

In sharp contrast, the MeV electron profile in Figure 2 shows no long-term effect of satellite absorption and is affected only at the inner edge of the trapped radiation region in the F-ring region before complete absorption occurs in the main rings. The 1979S2 microsignature [Fillius *et al.*, 1980; Simpson *et al.*, 1980a,b; Van Allen *et al.*, 1980a,b] near 2.5 planetary radii (1 R_S = 60,000 km) was a highly localized signature of absorption resulting from a probable near encounter with one of the co-orbiting satellites [e.g., Van Allen, 1984]. The absorption in the F-ring region is most likely due to multiple close encounters with distributed absorbers in that region [e.g., Cuzzi and Burns, 1988]. Thus the observed electron profiles are affected primarily by localized, strong absorbers.

Inward diffusion and acceleration produces a "inner core" population of MeV electrons in the inner magnetosphere which has distinctly different radial profiles as compared to the seed population in the outer magnetosphere at lower energies. Figure 4 shows radial

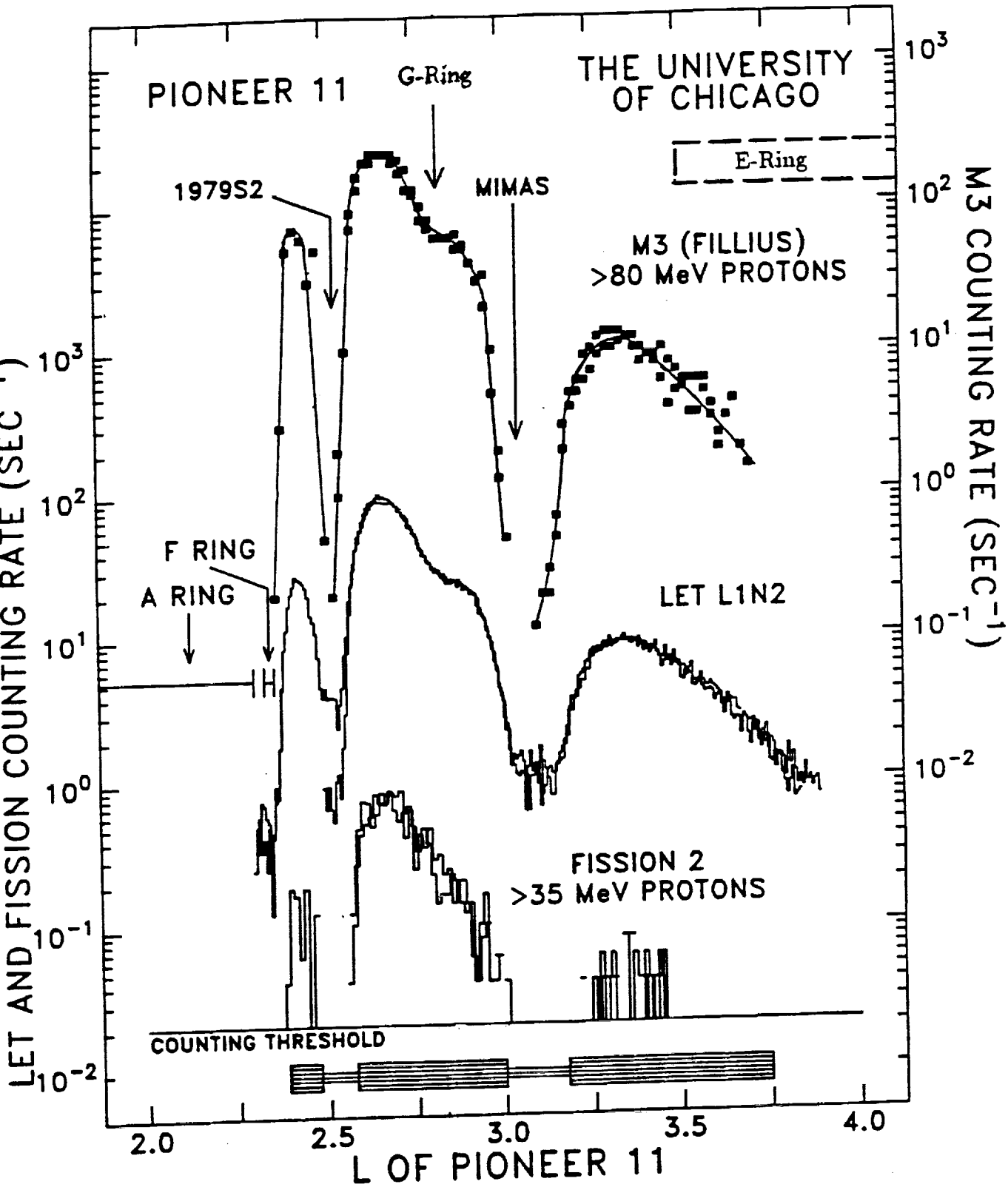

Figure 3: High energy proton profiles from Pioneer 11 at Saturn from the University of Chicago [Simpson *et al.*, 1980a,b, 1981] Low Energy Telescope (LET) rate "L1NL2" and Fission Cell, which both count protons above 30 MeV outside the satellite sweeping regions, and from the UC-San Diego M3 rate [e.g., Fillius *et al.*, 1980] for protons above 80 MeV.

profiles for integral counting rates of electrons above 0.040 and 0.56 MeV from the Pioneer 11 encounter [Van Allen *et al.*, 1980a; Van Allen, 1984]. While the electrons at 0.040-0.56 MeV show time dependent behavior outside the orbit of Tethys, the higher energy electrons show a monotonic increase inwards which is characteristic of steady inward acceleration for electrons counted by detectors with fixed energy thresholds. Just outside Tethys's orbit, the two profiles converge (note the different vertical scales) into a single "core" profile further inwards which is dominated by electrons above the higher energy threshold. The more rapid increases in the counting rates inside the orbit of Enceladus are unexplained but might be due to changes in the electron spectra, due to preferential absorption of higher energy electrons [Van Allen *et al.*, 1980c], or else to additional electron sources in the inner region.

The Voyager 2 encounter produced measurements for sub-MeV electrons which appear to be in conflict with the Pioneer 11 data and warrant further scrutiny. In Figure 5 the LECP (Low Energy Charged Particle Experiment) profiles from Krimigis and Armstrong [1982] are shown for 22-35 MeV electrons, $\geq$1.5-MeV electrons, and other rates for ions and CRAND protons in the region where the profiles in Figure 4 converge. In contrast to the Pioneer results, the LECP data indicate an increasing low energy electron component in the region inwards of Enceladus. One should note, however, that the background levels increase proportionately to the higher energy electron rate, such that electron contamination becomes dominant inwards of Mimas. A critical question for further investigation is whether the relatively low background levels at 4-5 R_S allow one to interpret the nominal profiles as being due to low energy particles. Since this question is critical to interpretation of the LECP data in terms of E-ring absorption effects (see accompanying section by L. Hood), the possibility of electron contamination is discussed further below.

Integral Intensities and Detector Responses

Electron intensities near a few MeV are high in the inner magnetosphere, although nowhere near peak levels two orders of magnitude higher at Jupiter, and there are potentially valid arguments [e.g., Van Allen *et al.*, 1980b,c] that various different types of measurements at Saturn may have been adversely affected by electron contamination in the inner region, particularly inwards of Mimas. A difficulty in evaluating such arguments is that no high resolution measurements of the electron spectra are available in the peak flux region below a few MeV. The best available compilation [Chenette and Stone, 1983] of electron spectra from integral detectors is shown on the left side of Figure 6 for the Mimas region, where contamination of the higher energy electron channels by CRAND protons was minimal. The right side shows the measured integral intensities above 10 MeV for protons and electrons from Pioneer 11 and Voyager 2 near the 2.7 R_S position of maximum intensity. The peak electron flux above 10 MeV and the peak proton flux above 600 MeV are taken from the more recent Pioneer 11 data analysis by Northrop and Fillius [1985], which takes into account the gradient-anisotropy effects relevant for the higher energy protons.

The usefulness of data from various Pioneer and Voyager detectors is determined in part by linearity of response to the intensity levels in Figure 6. Solid-state silicon detectors operate reliably at counting rate levels up to 10^4 cps and should have had reasonably good efficiency for measurements of electrons above five MeV and of protons at all energies. However, any such detector directly exposed to electrons incident with lower energies near 1-3 MeV would have been heavily saturated at peak intensities, unless the sensitive detector area was very small (e.g., $\leq 10^{-2}$ cm^2) and optimized for magnetospheric measurements at high

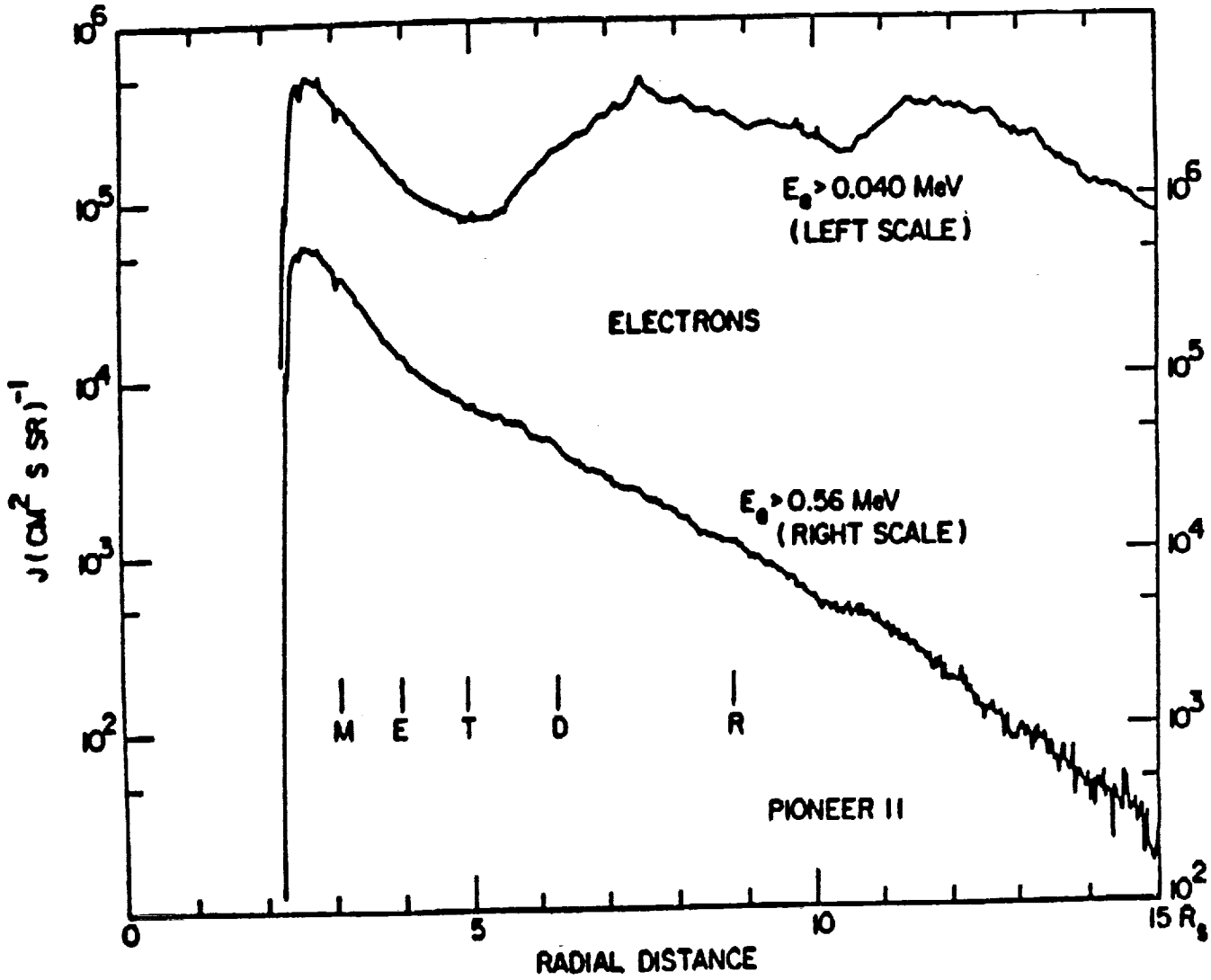

Figure 4: Inbound radial profiles at Saturn for electrons above 0.040 MeV and 0.56 MeV from the Univerisity of Iowa experiment on Pioneer 11 [Van Allen *et al.*, 1980a,b; Van Allen, 1984]. Note the convergence of the two profiles inwards from the orbit of Tethys, indicating that most electrons are above the higher threshold.

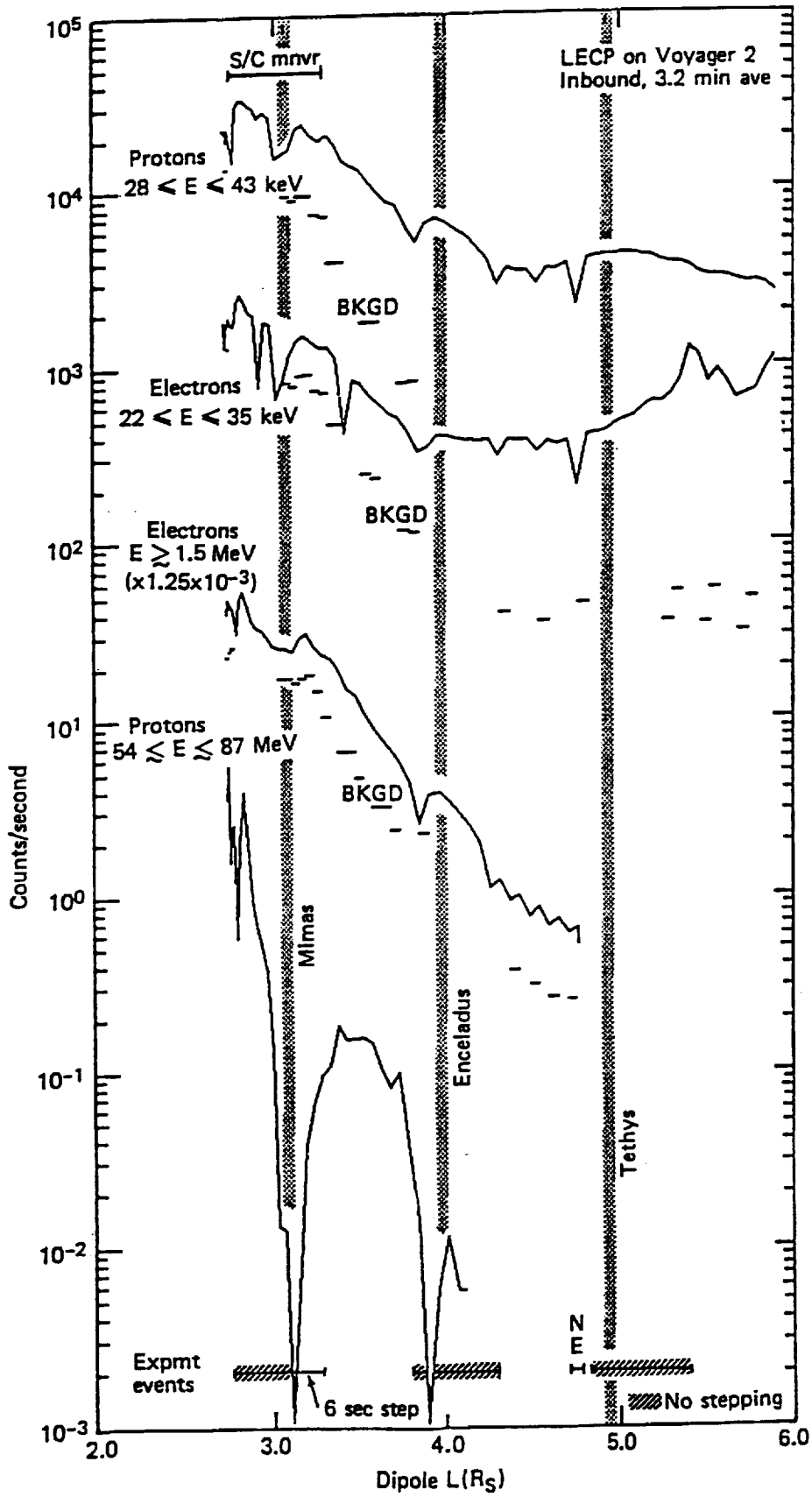

Figure 5: Inbound radial profiles from the Low Energy Charged Particle Experiment (LECP) on Voyager 2 for low energy protons, electrons, and for MeV electrons and high energy protons. [Krimigis and Armstrong, 1982]. The solid curves indicate the sector-averaged, nominal counting rates and the small, horizontal bars mark the background measurements for low energy particles as the instrument moves behind a sun shield during its rotational movement.

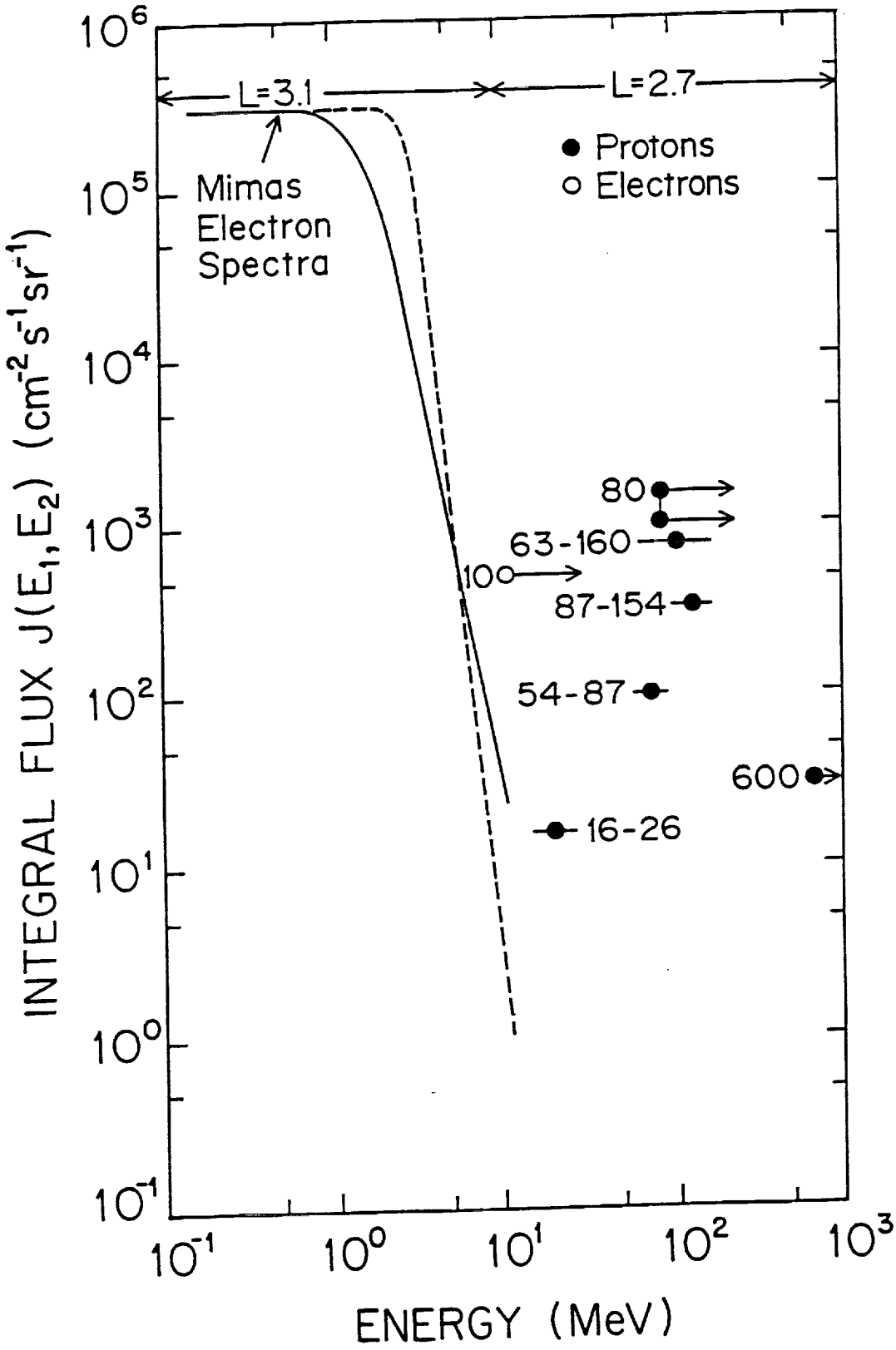

Figure 6: Compilation of integral flux spectra for electrons thresholds below 10 MeV in the Mimas region [Chenette and Stone, 1983] and for protons and electrons above 10 MeV near 2.7 R_S from Pioneer 11 and Voyager 2. The solid and dashed curves denote the range of uncertainty in spectra within the Mimas region. The proton fluxes near 2.7 R_S at 16-154 MeV and 63-160 MeV are from Krimigis and Armstrong [1982] and Vogt *et al.* [1982], respectively. The proton fluxes in the same region above 80 MeV are from the similar Pioneer 11 results of Fillius *et al.* [1980] and Van Allen *et al.* [1980a,b]. The fluxes above 10 MeV for electrons and above 600 MeV for protons come from the gradient-anisotropy analysis of Northrop and Fillius [1985]. Arrows indicate fluxes above single thresholds, while horizontal bars denote integral fluxes within finite energy bins.

flux levels. Typically, the detectors responding to electrons with higher energy thresholds were well-shielded by passive material against direct incidence by lower energy electrons. The unshielded detectors were either turned off, as for the Cosmic Ray Experiment (CRS) on Voyager 2 [Vogt *et al.*, 1982; Schardt and McDonald, 1983], or else counted steadily at a constant saturation level and did not significantly affect other detector counting rates. Although secondary radiation processes (i.e., bremsstrahlung) may have adversely affected counting rates of some single detectors, particular those with minimal shielding, such processes probably had negligible effects on rates for multiple detector coincidences. Four-fold coincidences were required for "7-17 MeV electrons" in the Pioneer-11 Chicago experiment [Simpson *et al.*, 1980a,b] and for "63-160 MeV protons" in the Voyager 2 Cosmic Ray Experiment, and electron background effects from accidental coincidences in single detectors were probably minimal for these rates. These two rates have interesting implications for the dust limit analysis as discussed further on.

"Pathological" Responses to MeV Electrons

The high electron intensities at low energies make it more probable that "pathological" response modes may become significant in some instruments. Early concerns about electron background were discussed by Van Allen *et al.* [1980b,c] and countered to some extent by the responsible experimenters for the more suspect instruments [e.g., Simpson *et al.*, 1980b, 1981], the high-order coincidence technique being the most effective defense against the contamination argument with respect to electron bremssstrahlung. Another source of contamination is leakage of energy electrons into the region of a sensitive detector via a small pathway through a passive shield which should otherwise stop the highest intensity electrons. A recent experimental calibration at Caltech has verified leakage of electrons near and above three MeV through the side of the Electron Telescope (TET) in the CRS experiment [R. Selesnick, private communication, 1989]. The measured pulse height spectra suggest that internal scattering of penetrating electrons contributes a major share of the background leakage signal in the detector. This result will have some impact, undetermined thus far, on the electron microsignature analysis of Chenette and Stone [1983].

A analogous issue is now raised regarding potential background response in the Low Energy Charged Particle Experiment [LECP] on Voyager 2. In this case the magnetic deflection system, used by LECP to determine allowed trajectories within the open aperture of the instrument for incidence of low energy electrons onto sensitive detectors (otherwise shielded against direct incidence), may have been rendered ineffective by internal scattering of the intense MeV electron flux also entering the front aperture. For both CRS and LECP, the usage of tungsten to stimulate secondary bremssstrahlung for high energy electron measurements (CRS) or for passive wall construction (LECP) would have greatly amplified the leakage effects, because of tungsten's relatively high efficiency (near 50 percent) for backscattering of MeV electrons. Although the LECP instrument uses a sun shield in one of its eight rotational sectors to block the front aperture and allow measurement of penetrating background rates, this shield may have largely attenuated the primary background component, electrons with peak differential fluxes near the stopping energy (1.3 MeV) of the shield, and produced low background readings in the data of Figure 5 for the inner magnetosphere. Due to its potentially adverse impact on the accompanying E-ring analysis of L. Hood, the LECP background response warrants further scrutiny.

The Pioneer and Voyager measurements in the inner magnetosphere of Saturn are not

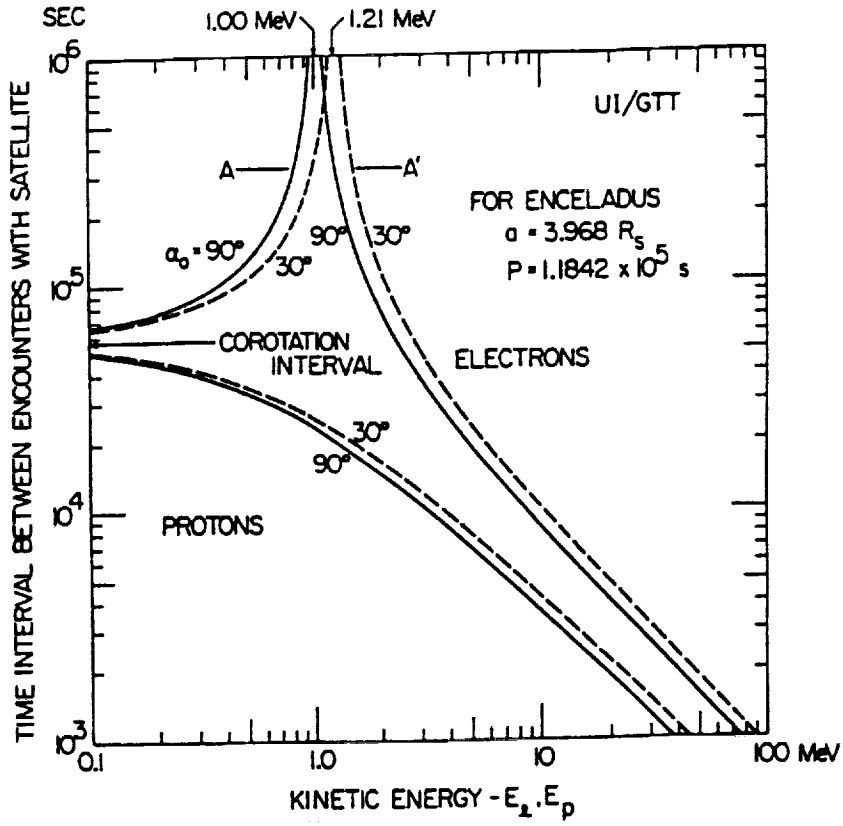

Figure 7: Satellite encounter times versus energy for electrons and protons drifting longitudinally in the radial orbit of Enceladus at equatorial pitch angles of 30 and 90 degrees [Van Allen *et al.*, 1980c]. For electrons and lower energy protons these are also the times for snowplow (e.g., total) absorption by Enceladus.

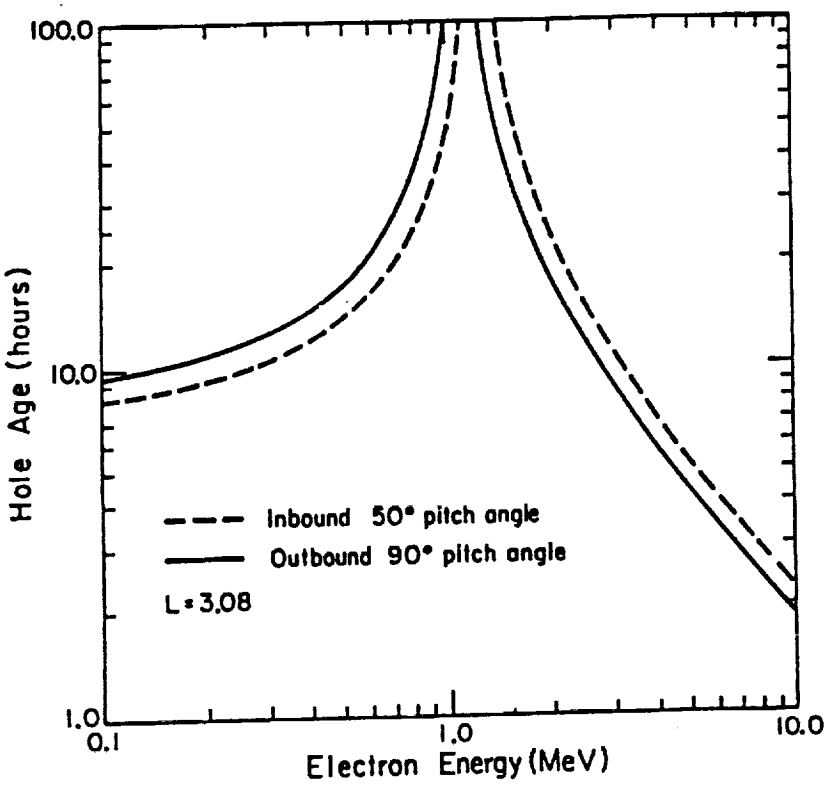

Figure 8: Energy-dependent times for absorption of electrons at pitch angles of 50 and 90 degrees at the orbit of Mimas [Vogt *et al.*, 1982]. Note that the drift resonance energies are similar to those for Enceladus in Figure 7.

sufficient to resolve the differential shape of the Saturnian electron spectrum in the critical energy region near 1-2 MeV where drift resonance effects are expected. Figure 7 shows the calculated loss times from Van Allen *et al.* [1980b,c] of electrons in the sweeping region of Enceladus. The large increase in loss time near 0.9-1.3 MeV corresponds to the energies at which electrons have minimal relative drift in magnetic longitude with respect to Enceladus. Although the resonance would significantly distort the measured electron spectrum at 0.1-3.0 MeV, electrons at other energies and protons at all energies have finite loss times governed by energy-dependent velocities for longitudinal drift relative to the satellite and are unaffected. The flatness of the integral electron spectrum up to 1-2 MeV in Figure 6 could be accounted for by a resonance feature in the differential spectrum as predicted. Since inwardly diffusing electrons are accelerated, the resonance peak of the electrons getting by Enceladus moves to a higher energy with decreasing L towards Mimas's orbit, whereupon, sweeping by Mimas introduces a new resonance as shown in Figure 8 from calculations by Vogt *et al.* [1982]. Similar resonances would be produced by satellites at the orbits of Tethys and beyond.

The pathological interpretation of the LECP data in Figure 5 is then that the differences between the nominal counting rate levels and the background levels are due solely to absorption of the resonance peak electrons by the LECP sun shield during the background measurement. In this interpretation the nominal rates for 22-35 keV electrons and for 28-43 protons are dominated by internally-scattered MeV electrons inwards of Enceladus. The background level also increases radially inward from Enceladus where a significant fraction of the resonance electrons are above the energy required to penetrate the sun shield, and acceleration increases this fraction with decreasing L. Between Tethys and Enceladus the bonafide low energy particles may be decreasing in intensity radially inward as the background component increases, so the total nominal rates are nearly constant. The constancy of the background rates for 22-35 keV at 4-6 R_S suggests that these rates may be dominated by other radiation components in this region and beyond.

A possible "smoking gun" for the above pathology is found in the LECP electron spectra reported by Krimigis *et al.* [1983]. These spectra were measured by LECP instruments for both Voyager encounters with Saturn and are reproduced here as Figure 9 (their Figure 12). In the outer magnetosphere ($L \geq 10$) both sets of spectra are either exponential or power law at energies up to one MeV, as one might expect for the usual magnetospheric processes. In the Voyager 2 data at $L = 4 - 7$, however, one sees very unusual spectra with power laws at 30-100 keV and large humps in the spectra at 100-1000 keV. The absence of such features at comparable positions in the Voyager 1 data suggests a time-dependent effect, perhaps analogous to that seen in the Pioneer 11 electron data.

The innermost spectrum at $L = 4.2 - 5.4$ shows a local maximum quite near the energy predicted by Van Allen *et al.* [1980c] for drift resonant electrons diffusing past the Enceladus region. Note that the flux falls rapidly at 1-10 MeV as also expected. In the absence of published spectra with better spatial resolution, we can only speculate that the maximum grows larger inwards of Tethys's orbit (4.9 R_S). The other Voyager 2 spectrum for $L = 6.9 - 5.9$ R_S does not show the same peak structure but may be partially affected by a Dione (6.3 R_S) drift resonance.

Although no similar LECP data are given inwards of Enceladus, probably due to uncertainties in background corrections, we further speculate that the resonance peaks in the electron spectra become totally dominant there, and that the low energy fluxes cannot be measured without quantitative corrections for background from electrons in these peaks. In

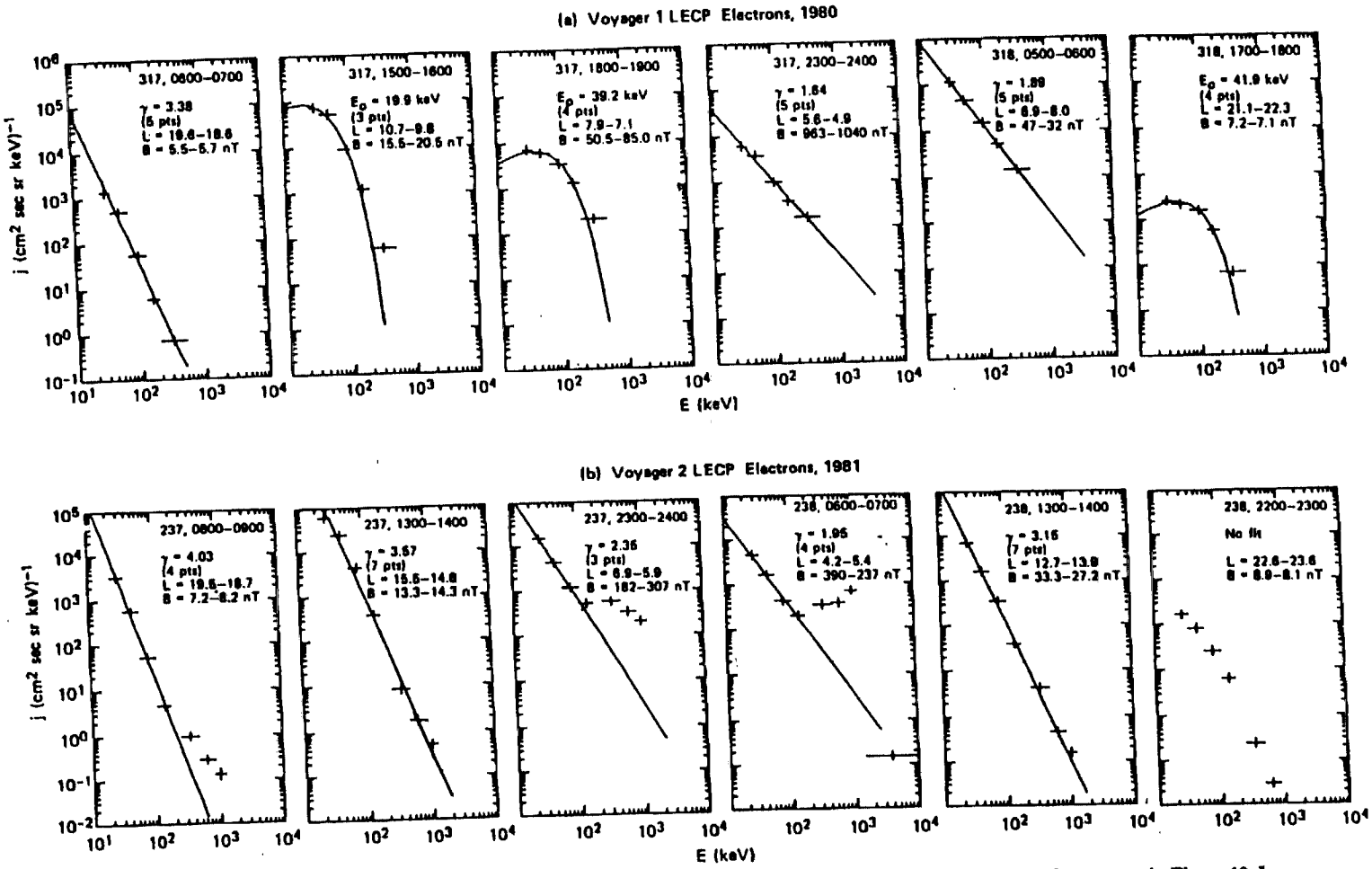

Fig. 12. Differential electron spectra for (*a*) Voyager 1 and (*b*) Voyager 2 with each point plotted at the geometric mean, as in Figure 10. In Figure 12*a* the five Voyager 1 channels have been fitted by either a power law in energy or an exponential with the indicated parameters. In Figure 12*b* up to seven points are fit, due to the availability of detector γ, with the indicated power law indices. In each panel the initial and final values of L and B over the indicated time interval are noted.

Figure 9: Differential electron spectra from the Low Energy Charged Particle Experiment (LECP) on Voyager 1 and Voyager 2 [Krimigis *et al.*, 1983]. Note the departures from power-law spectra in the two center panels for Voyager 2.

the intermediate region at $4 - 5$ R_S, where local minima appear in the radial profiles for low energy electrons and ions, the electron spectra are probably an even mixture of the soft, low energy component and the high energy, resonance component. The apparent inward increase from the transition region of the low energy counting rates may simply reflect increasing background levels from the now dominant resonance component.

Differential Spectra for Protons

Differential flux measurements of proton energy spectra could provide a sensitive measure of absorption in diffuse dust layers near the ring plane, since the proton loss rate in dust increases with decreasing energy below 300 MeV due to ionization energy loss. In Figure 10 we compare the calculated CRAND source spectrum for protons from Cooper [1983] with the very limited data on spectral measurements from Pioneer 11 and Voyager 2. Relative to the nearly flat source spectrum below 100 MeV, the measured spectra from the Voyager 2 Low Energy Charged Particle (LECP) experiment [Krimigis and Armstrong, 1982] show strong depletion of low energy protons at L = 2.73, possibly indicating dust-dominated ionization losses in that region. A comparable differential flux at 63-160 MeV is also available from the Voyager 2 Cosmic Ray (CRS) experiment of Vogt *et al.* [1982]. CRS proton measurements at lower energies (48-63 MeV) show apparent increases of differential fluxes from higher energies, but spectrum-dependent corrections for electron background make this determination highly uncertain [Schardt and McDonald, 1983]. We assume that the LECP data better represent the actual shape of the spectra below 100 MeV.

Overall, the differential fluxes in Figure 10 are consistent with a CRAND source spectrum and energy-dependent losses below 100 MeV from interactions with dust. The LECP spectra at 10-100 MeV are a reasonable match to a theoretically derived spectrum [Schardt and McDonald, 1983] of the form $J(E) \propto E^{1+\gamma}$, where $\gamma \approx 0$ approximates the source spectrum below 100 MeV. At higher energies, from 80 MeV to above 600 MeV, the integral flux data from Pioneer 11 [Fillius *et al.*, 1980; Northrop and Fillius, 1985; Van Allen *et al.*, 1980b] are consistent with the indicated differential spectrum ($\gamma \approx -3$) in Figure 5 and with the CRAND source spectrum.

Since radial diffusion broadens the effective region for observable effects on the proton spectra, it is plausible that the Voyager 2 spectra at 2.73 R_S were affected by absorption occurring further outwards in the G ring. However, the Voyager 2 LECP found similar spectra at 3.4 R_S, although with less depletion near 20 MeV, so one cannot rule out local absorption effects from the measured spectra which actually appear quite consistent with expected losses in dust. One might speculate that the dust densities are just high enough to affect the lower energy protons, but that the integral intensities of higher energy protons are minimally affected. Since our CRAND modeling of radial profiles for the latter shows no significant dust effect, the marginal column densities for lower energy losses would correspond to the "worst case" limits for 100-MeV protons. These limits are relative high (10^{-7} gm/cm^2) in the E ring, and the same limits would give observable effects on the radial profiles near 2.7 R_S in contrast to the modeling results. Alternatively, some other explanation may be found for the spectra which is unrelated to dust effects (e.g., low energy anomaly in the CRAND source spectrum, unaccounted-for effects of background contamination?).

Pitch Angle Anisotropies

Anisotropy measurements for the pitch angle distributions of trapped protons are also

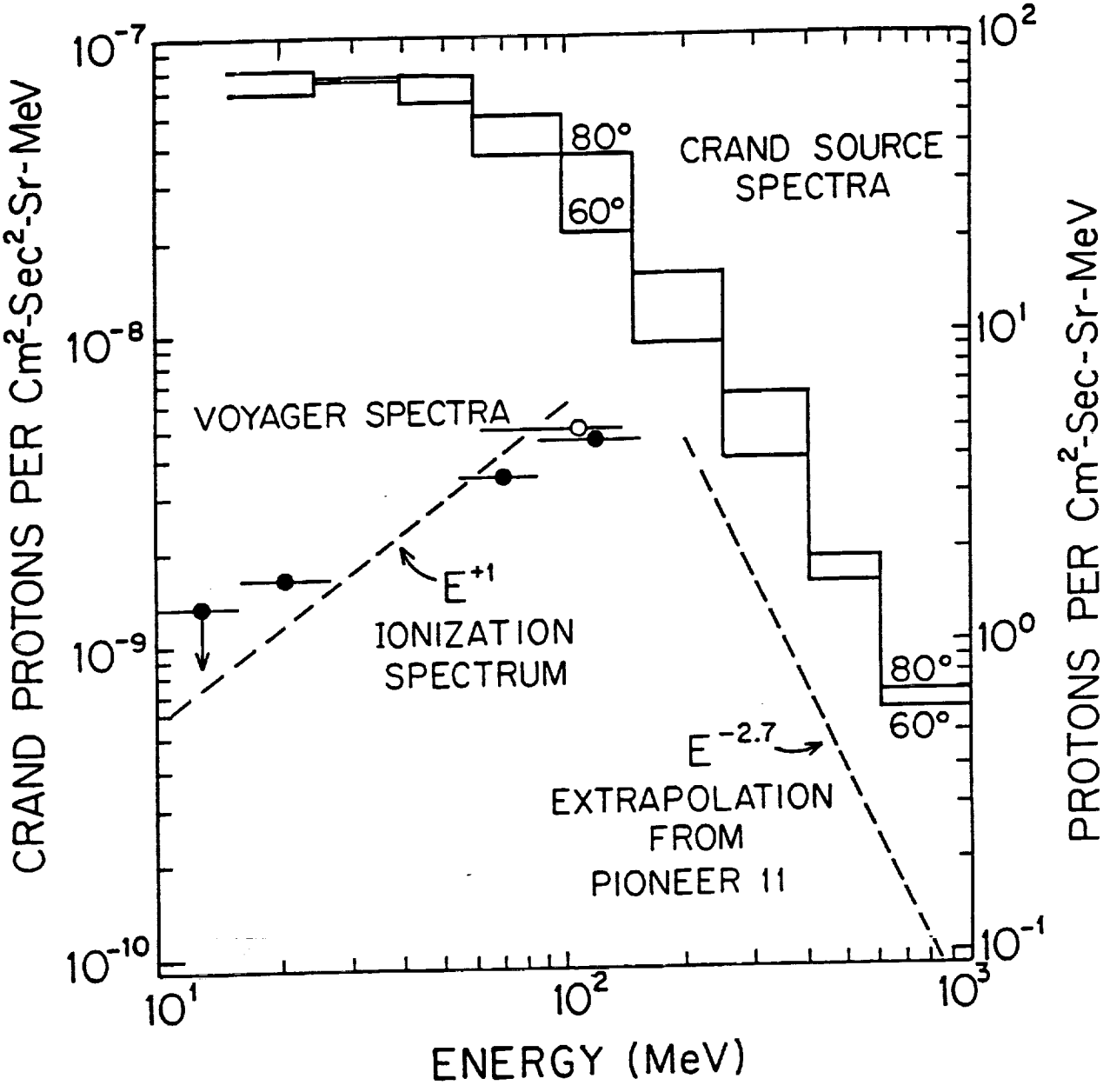

Figure 10: Calculated [Cooper, 1983] and measured (dark circles from Krimigis and Armstrong [1982]; open circle from Vogt *et al.*, 1982) differential energy spectra for CRAND protons at L $\approx$ 2.7. The higher energy, dashed spectrum is extrapolated from the integral fluxes above 80 MeV and 600 MeV in Figure 6.

sensitive to the presence of diffuse dust or larger aggregates of co-orbiting material near the ring plane. Voyager dust impact data [Scarf *et al.*, 1982, 1983] indicate that detectable dust layers at Saturn are confined within a few thousand kilometers of the ring plane. Protons with large equatorial pitch angles α_0 at the ring plane have larger pathlengths through a layer of uniform thickness and therefore have greater losses. The absorption of the equatorially trapped proton population becomes especially prominant when observed in the CRAND proton population. Such protons are nominally expected [Blake *et al.*, 1983] to have preferentially higher injection rates for large values of α_0.

In principle, the correlation of anisotropies and differential energy spectra should allow differentiation between absorption effects due to dust and to other absorbers, including major satellites. Declining LECP spectra below 100 MeV and reduced CRS anisotropies are jointly indicative of absorption in a layer of small dust particles, where the spectral effect arises from slow energy losses as compared to catastrophic single impacts with large particles (i.e., radii much larger than ten centimeters). The random distribution of larger particles (e.g., moonlets up to kilometers in size) over a wide radial range in a vertically thin layer can also produce anisotropies like those observed, but only the smaller particles produce the spectral effect.

Figure 11 shows a Voyager 2 measurement of proton anisotropies for for 63-160 MeV protons as reported by Schardt and McDonald [1983]. Ratios of inbound and outbound fluxes at different magnetic latitudes were used to determine the "pancake" distribution parameter n for the differential distribution $j(\alpha_0) \propto sin^n\alpha_0$ of directional flux near the ring plane. The largest values of n (i.e., more anisotropic fluxes) were found in the highest proton flux regions, as expected for nominal geometry of the CRAND source [Blake *et al.*, 1983], while low values (i.e., more isotropic fluxes) were found in the vicinity of the G-ring, Mimas's orbit, and in the E-ring region beyond 3.3 R_S. In the latter region, the radially outward decrease in n is suggestive of a strong E-ring effect but may have other explanations.

One such explanation was first advanced by Cooper [1983], who noted that re-absorption of CRAND-parent neutrons would occur preferentially for emission from ring source regions at more tangential angles with respect to the ring plane. Figure 12 shows Cooper's calculations for the dependence of CRAND injection efficiency (i.e., the injection coefficient) on equatorial pitch angle with a simple, thick slab model the parent neutron source in the main rings. Although this calculation underpredicts the anisotropy of the injected protons inwards from 3.3 R_S, where the discrete nature of the neutron-emitting bodies in the rings [Blake *et al.*, 1983] accounts for the largest anisotropies observed, it does predict decreasing injection efficiency at large distances for protons with large equatorial pitch angles. This effect arises because (1) the parent neutrons have increasing slant pathlengths for escape from the source slab, and (2) the radial distance from the source to the injection point increases faster for injection near the equatorial plane at large L than at high latitudes, where injection sites remain directly over the rings for the smallest equatorial pitch angles. Whether this totally explains the isotropization of protons in the E-ring region is unclear, but more realistic modeling of the ring source would be helpful to resolve this question. What is surprising is that no one, myself included, has addressed this rather obvious problem since Schardt and McDonald reported the anisotropy results in 1983.

The pitch angle distributions of injected protons should be sensitive to size distributions and vertical positions of neutron-emitting bodies within the main rings, where the typical sizes of such bodies are of order one meter in radius as compared to 10-100 meters for the ver-

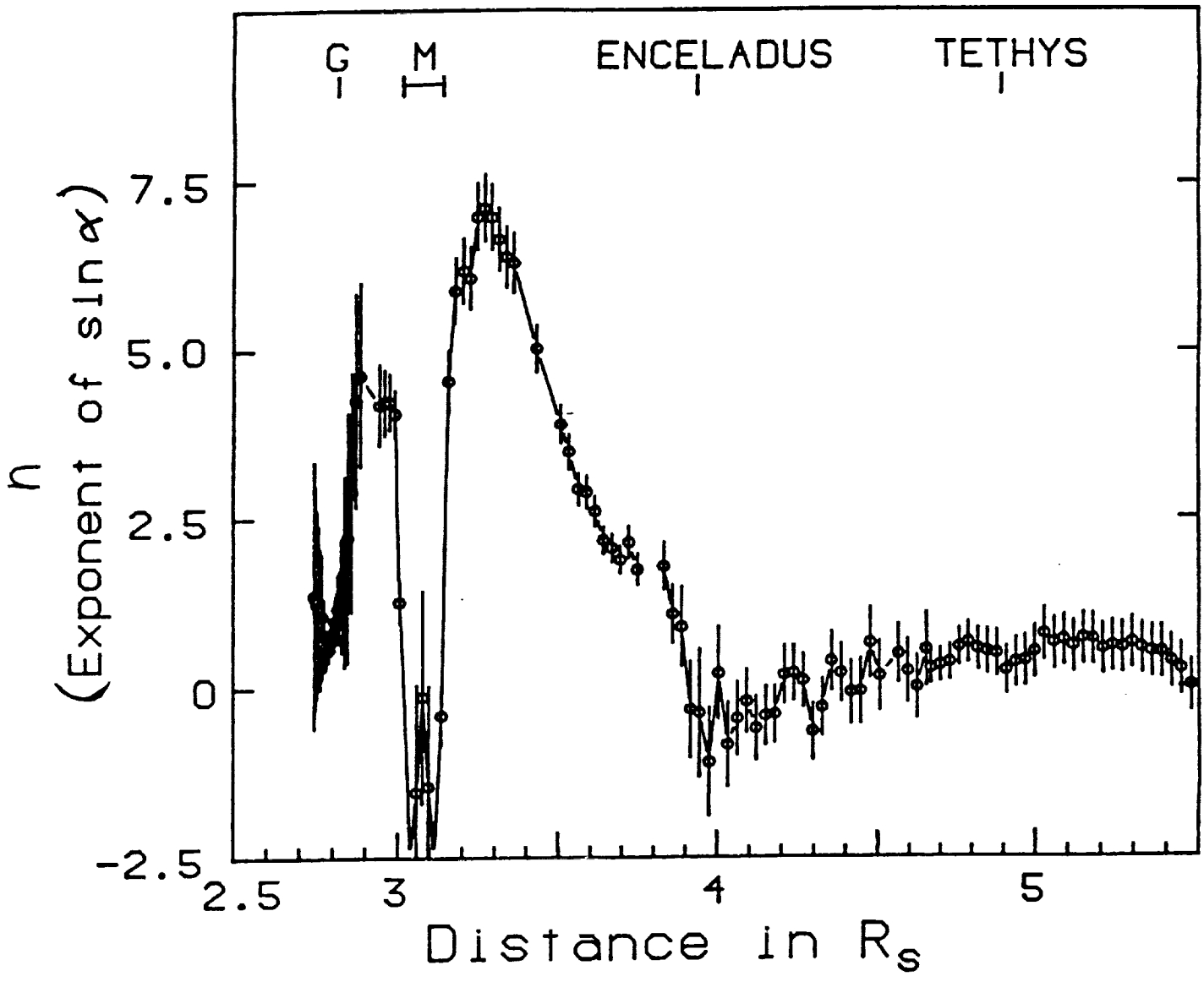

Figure 11: Anisotropy index n for 63-160 MeV protons from the Cosmic Ray Experiment (CRS) on Voyager 2 [Schardt and McDonald, 1983]. Large values indicate relatively more equatorially trapped protons, while smaller values arise for more isotropic distributions.

tical ring thicknesses [Tyler *et al.*, 1982]. At some radial distance, dependent on the ratio of interparticle separation distances and the vertical dispersion scale, one should expect strong reabsorption of tangentially scattered neutrons, perhaps leading to the observed effects beyond 3.3 R_S. At higher proton energies, above a few hundred MeV, this effect should become more pronounced, since scattering angles decrease with increasing secondary neutron energy. In this regard, improved measurements of CRAND proton energy spectra and anisotropies in this region by Cassini might therefore used to probe the internal structure of ring particle distributions in rough analogy to an nuclear scattering experiment in high energy physics. Sophisticated monte carlo codes, originally developed for work in high energy physics, can be used to explore these possibilities.

High Energy Electrons

A unique signature of diffuse dust in regions of peak proton intensity would be the presence of highly relativistic electrons with radial intensity profiles roughly approximating those of the parent CRAND protons. Since longitudinal drift rates of both protons and electrons scale roughly with kinetic energy, one expects very low flux levels for electrons above 10 MeV as observed [Chenette and Stone, 1983] in satellite regions where the proton fluxes are low. The electron and proton fluxes may be much higher elsewhere in the absence of strong absorption, but only if local *in-situ* sources are active. Since CRAND already provides the required source for the protons, nuclear interactions of the protons above 300 MeV would provide a source of high energy electrons via pion production at a level proportional to the proton fluxes and to the column density of diffuse dust. Upon injection, the pionic electrons would have energy spectra extending into the 10-100 MeV range, the mean pion-muon decay energy for electrons being near 50 MeV. If the trapping lifetimes of these electrons were limited largely by radial diffusion, as for the protons, the observable spectra of the time-averaged electron population could be comparable in shape to the injection spectra, while a more significant loss rate from dust interactions would tend to soften the time-averaged spectra due to the increasing losses from bremsstrahlung at higher energies. In either case one would expect significantly flatter spectra above 10 MeV from the dust source than are observed in satellite regions, where inwardly diffusing electrons would dominate the integral fluxes below 5-10 MeV, and the local source component would be rapidly reabsorbed.

Experiments which do not discriminate between penetrating protons and the higher energy electrons can produce highly ambiguous results as seen in the "7-17 MeV Electron" profiles in Figure 13 from the University of Chicago's charged particle experiment onboard Pioneer 11 [Simpson *et al.*, 1980a,b, 1981; R. B. McKibben, unpublished data, 1988]. These profiles may be considered to be a mixture of contributions from electrons at energies above 7 MeV and from protons above 30 MeV. The electrons are dominant in radial zones of proton absorption by Janus/Epimetheus near 2.5 R_S and in the vicinity of the F-ring region, while the protons account at least partly for the peak counting rates near 2.4 R_S and 2.7 R_S. The large change in counting rates in the vicinity of the absorption regions is probably due to rapid changes in the electron intensities over the intervening four-hour interval between inbound and outbound observations [Fillius *et al.*, 1988].

The outbound drop in electron intensity over a wide radial range in Figure 13 reveals the rising shoulders of profiles for more stably trapped particles which are strongly absorbed within the satellite and ring regions. An outstanding question is the composition of the stably trapped particles in the peak intensity regions. The possibility remains that electrons

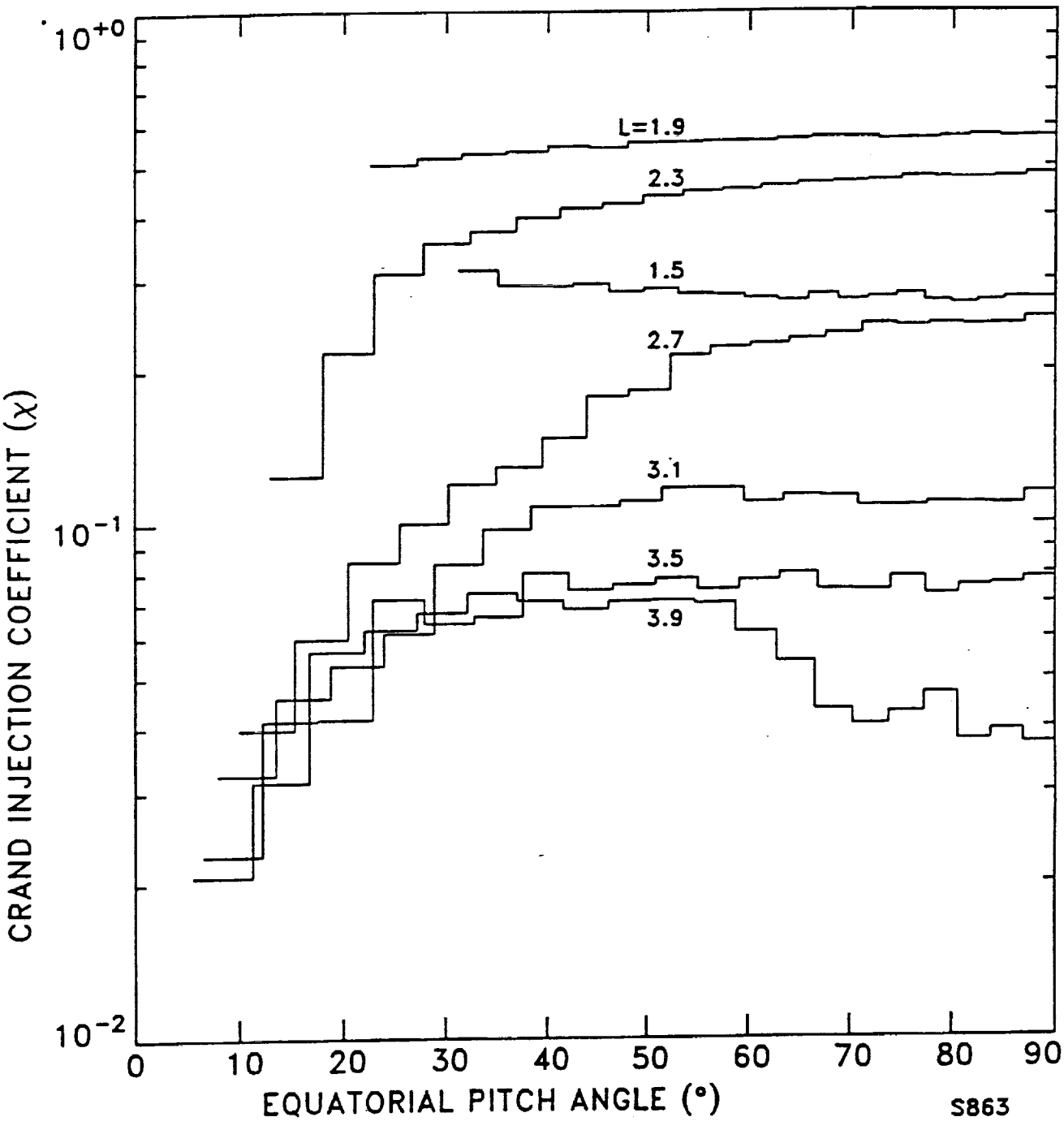

Figure 12: Calculated injection coefficients versus equatorial pitch angle for CRAND protons at selected radial positions [Cooper, 1983]. These coefficients were calculated for parent neutrons emitted from sources in the A and B rings, modeled as a uniformly thick annular disk at 1.5-2.3 R_S. Note the reduced injection at large pitch angles near Enceladus and beyond.

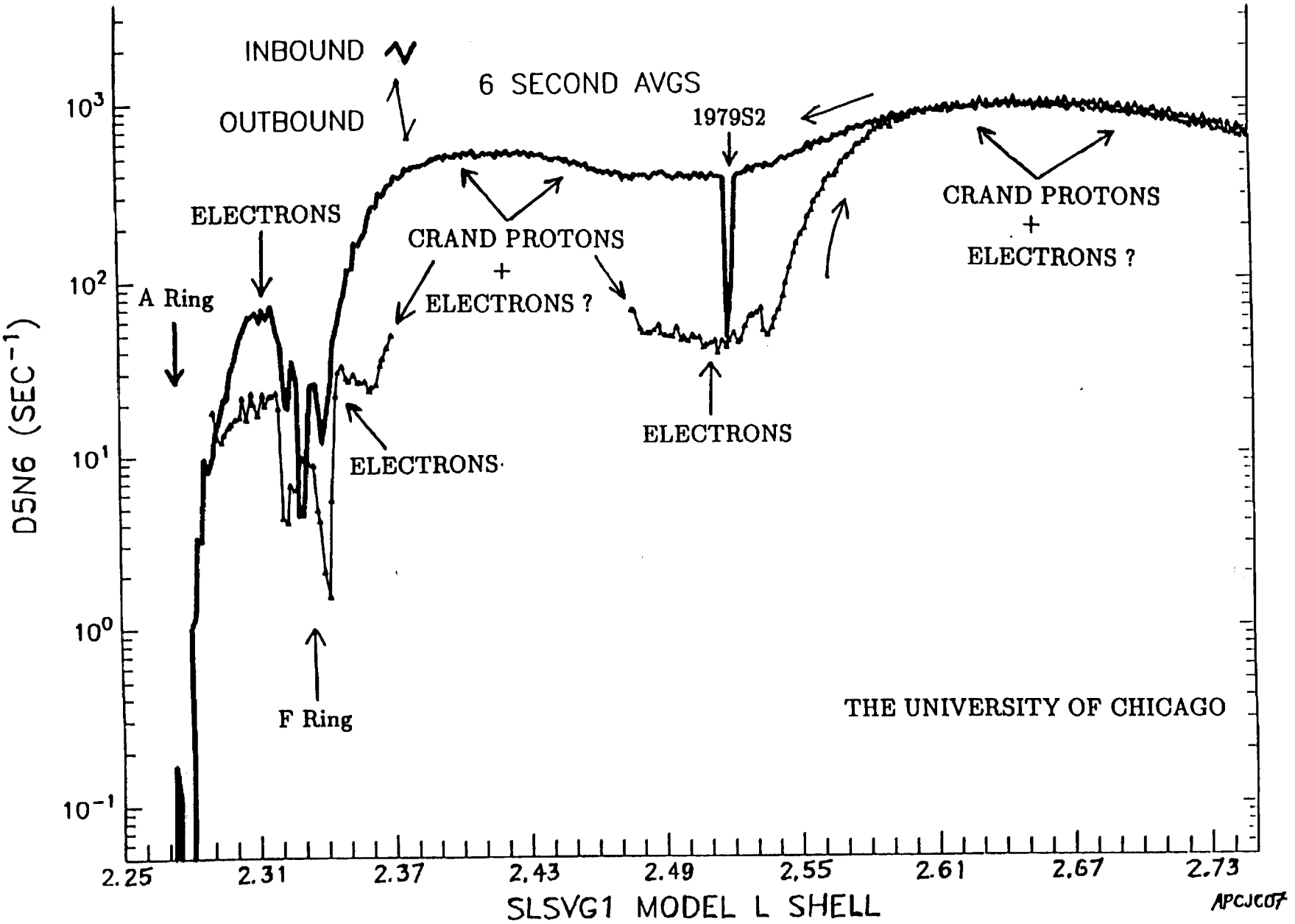

Figure 13: Inbound and outbound radial profiles for "7-17 MeV Electron" counting rate from Pioneer 11 [Simpson *et al.*, 1980a,b; R. B. McKibben, private communication, 1988]. As indicated, this rate may respond to a mix of nominal electrons and protons above 30 MeV in regions of high proton intensity. The electron response is dominant in profiles for the satellite and F-ring regions, which show large drops in intensity on the outbound pass due to a magnetospheric perturbation [Fillius *et al.*, 1988].

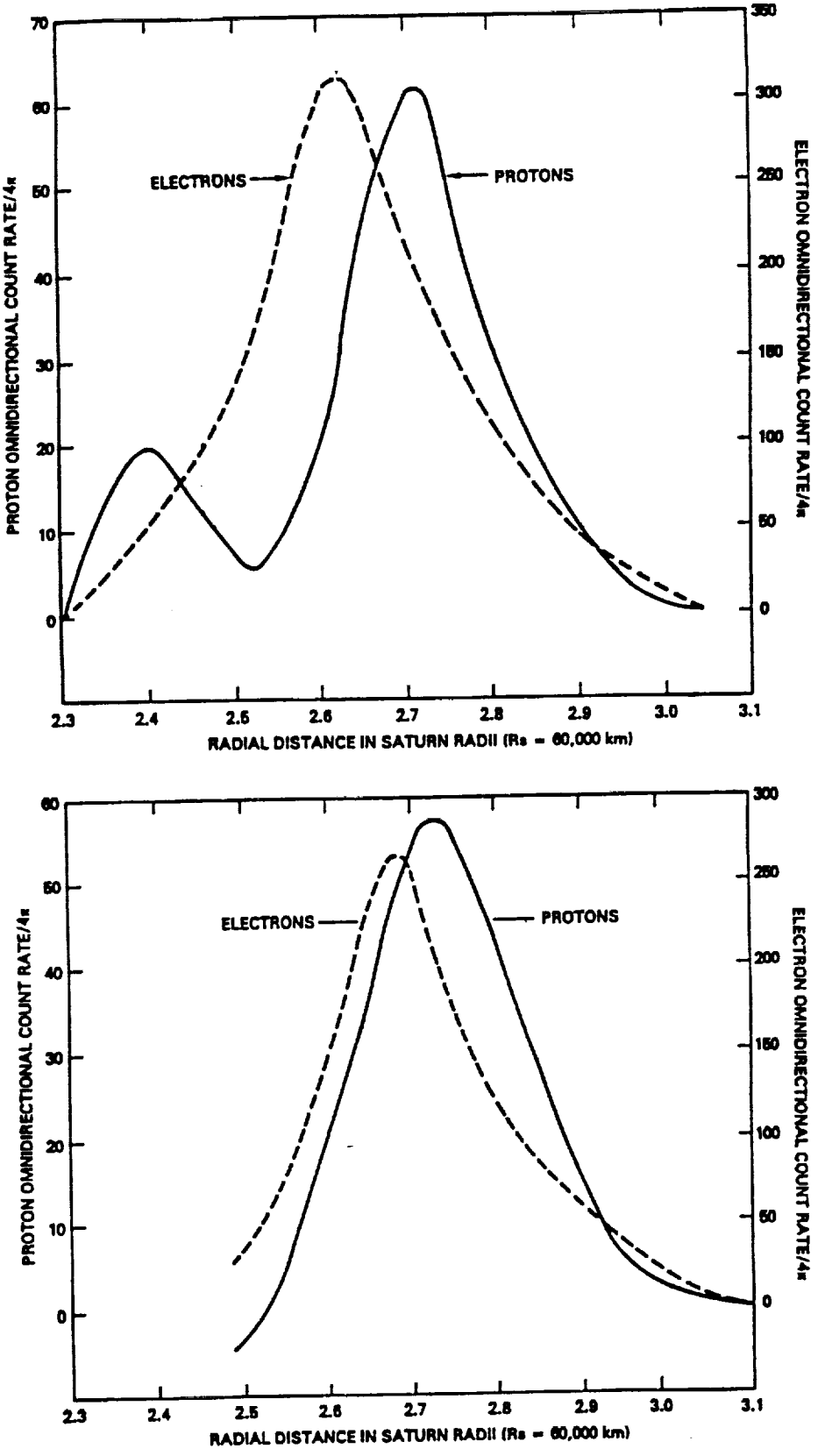

Figure 14: Inbound (top) and outbound (bottom) radial profiles from Pioneer 11 for electrons above 10 MeV and protons above 600 MeV, as determined by the gradient-anisotropy analysis of Northrop and Fillius [1985]. Note the significant inbound-outbound asymmetry in the electron flux profiles inwards of 2.6 R_S which is similar to that observed for the "7-17 MeV electrons" in Figure 13.

at 10-20 MeV dominate the counting rates in these regions. In this case the peak intensity regions observed outbound might be partially, if not totally, dominated by higher energy secondary electrons from the proton-dust interactions. Although the pionic electrons would be produced with average energies near 50 MeV from pion-muon decays, long term trapping and radiation losses in the dust might produce an equilibrium population of electrons with lower average energies in the 10-30 MeV range. Thus this secondary population might contribute substantially to the 7-17 MeV electron counting rates. On the other hand, we cannot yet rule out the possibility that this rate is entirely due to protons without new measurements by Cassini.

Although the high energies of the pionic electrons and their proton parents make discrimination between the electrons and protons difficult, the gradient anisotropy effect has already been used in the Pioneer 11 data analysis [Fillius and McIlwain, 1980; Northrop and Fillius, 1985] to estimate this separation and to establish the presence of electrons at energies above 10 MeV with radial intensity structure similar to that of protons above 600 MeV. The electron fluxes are separated from those of protons by the negligible east-west anisotropies of the electrons in comparison to the very significant anisotropies observed for protons above 600 MeV. The latter have large gyroradii which offset guiding centers by 10^3 km for protons measured in regions of large radial intensity gradients. Figure 14 shows the deconvolved profiles from Northrop and Fillius [1985] for the electron and proton components as measured (a) inbound and (b) outbound by Pioneer 11. Although the electron intensities in the 2.5 R_S region of satellite absorption show a large outbound drop in intensity similar to that of the "7-17 MeV Electrons" in Figure 13, the intensity peaks of both the electrons and the protons change little in magnitude or position between inbound and outbound observations and are probably associated with stably trapped populations. Although proton-dust interactions were not considered by Northrop and Fillius in their discussions of potential electron sources, it entirely possible that the electrons near 2.7 R_S are pionic in origin and therefore are also strongly indicative of a radially extended diffuse dust layer not unlike the more easily observable E-ring material beyond the orbit of Mimas.

Microsignatures

Among the most controversial aspects of the Pioneer and Voyager encounters were undoubtably the simultaneous detections of microsignatures by different experiments on the same spacecraft in the orbital region (also called the macrosignature region) of Mimas. Van Allen *et al.* [1980c] argued that the single Pioneer microsignature for Mimas (observed inbound) could be explained by the effect of MeV electron response in all affected data channels to a direct drift shadow from Mimas, located 56 degrees eastward from Pioneer 11 in magnetic longitude (MeV electrons drift westward). In rebuttal, Simpson *et al.* [1980b] argued strongly that the observed microsignature, evident in Figure 15 from counting rates nominally for 0.5-1.8 MeV protons and 7-17 MeV electrons, could not be explained by electron contamination.

The so-called "L1NL2" counting rate for the MeV protons shows highly aliased response in some locales within the Saturnian magnetosphere. The high intensity peaks, evident in Figure 3 for the nominal MeV (L1NL2) proton profile, have been attributed [Simpson *et al.*, 1981; Cooper, 1983] to side-penetration of the associated detector by CRAND protons at much higher energies, while the low but finite counting rates in the Mimas region are still attributed to MeV protons, based solely on the proton-like nature of the measured energy

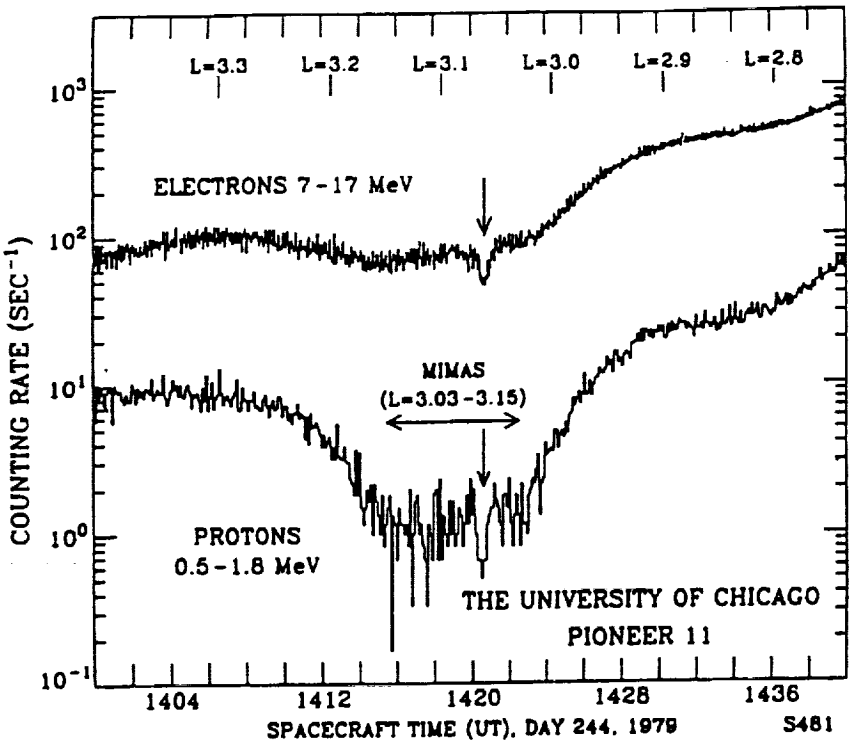

Figure 15: The "Mimas" microsignature as observed inbound in the "7-17 MeV electron" and "0.5-1.8 MeV proton" counting rates from the University of Chicago experiments on Pioneer 11 [Simpson *et al.*, 1980a,b]. Increases in both rates on each side of the Mimas sweeping region are most likely due to background from high energy protons. This feature was also detected in the Pioneer 11 data of Van Allen *et al.* [1980a,b,c]. No corresponding feature was detected outbound.

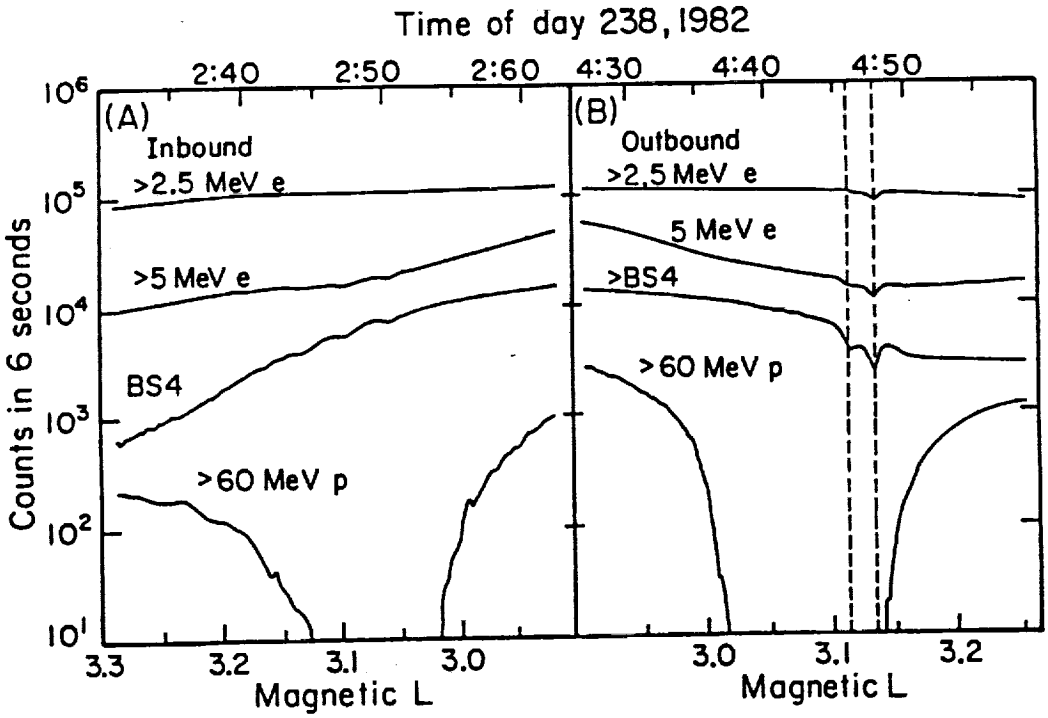

Figure 16: Inbound (left) and outbound (right) counting rates in the Mimas region from the Voyager 2 Cosmic Ray Experiment (CRS) [Vogt *et al.*, 1982; Chenette and Stone, 1983]. The "BS4" rate is a double coincidence for detectors sensitive to 2.5 MeV and 6.5 MeV electrons. The "5 MeV electron" rate is also sensitive to electrons near three MeV due to side penetration response in the CRS Electron Telescope [R. Selesnick, private communication, 1989]. Spacecraft maneuvers may have affected the inbound profiles, while the "Mimas ghost" microsignature is observed only outbound near the outer radial limit of Mimas's eccentric orbit, which appears to sharply define an absorption boundary for the high energy protons.

deposits in the detectors. On the other hand, it is clear that the L1NL2 rate will count electrons at some level, since this rate is correlated to the inbound-outbound flux decrease for electrons in the 2.5 R_S region, although no pulse height data are available from there. There was no appreciable decrease in the Mimas region. Ongoing analysis of calibration data from laboratory tests of a similar detector with a high flux, beta electron source [J. F. Cooper and J. P. Wefel, unpublished data, 1989] may produce a more definitive evaluation of the electron background problem for this detector.

Voyager 2 detected a single, outbound microsignature, shown in Figure 16, in the Mimas region in both electron [Vogt *et al.*, 1982] and low-energy ion [Carbary *et al.*, 1983] channels, this time when Mimas was 147 degrees west of the observing spacecraft. This was interpreted by Chenette and Stone [1983] as supporting the original view of Simpson *et al.* [1980b]. Chenette and Stone further proposed that the observed microsignatures probably arose from near encounters with 100-km clumps of co-orbiting material which may have been widely distributed throughout the macrosignature region to give the observed, fifty-percent probability of detection as microsignatures. Carbary *et al.* also found a single inbound microsignature at the orbit of Enceladus in low energy ion and MeV electron data. They also attribute the Enceladus feature to clumping of co-orbiting material, perhaps associated with the E-ring. The evidence for clumping is even more dramatic in the F-ring, where Cuzzi and Burns [1988] have argued that three of the five F-ring microsignatures, observed by Pioneer 11 experiments [Simpson *et al.*, 1980a,b; Van Allen *et al.*, 1980a,b] and shown in Figure 17, could not have been produced by the F-ring itself and must have arisen from random encounters with clouds of debris in the general vicinity.

Interpretation of the microsignature observations may lead to new planetary science but also indicates potentially grave hazards for the Cassini orbiter in the satellite regions. The common "horseshoe" orbits of the fragmented satellites Janus and Epimetheus at 2.52 R_S are the most easily observed example of stable orbital configurations in which many bodies can occupy the same radial zones by means of N-body gravitational interactions [e.g., Cuzzi and Burns, 1988; J. Burns, private communication, 1989]. Assuming that no residual problems remain with the microsignature observations, one is forced to conclude that large numbers (e.g., thousands) of localized debris clumps may co-orbit with the F-ring and the larger satellites. On the other hand, some of the microsignature data may be subject to "pathological" responses to high intensity background from MeV electrons, viz-a-viz the concerns of Van Allen *et al.* [1980b,c], so further experimental and analytical effort would be appropriate to evaluate the microsignature data and the likelihood of such responses.

3. CRAND Models for the Proton Observations

The thesis work of Cooper [1983] provides our starting point for modeling the CRAND proton observations in the inner magnetosphere of Saturn. This work modeled the main rings as a solid slab of material with an average column density of 100 gm/cm^2, a value in reasonable agreement with Voyager measurements from microwave-radio [Tyler *et al.*, 1982; Marouf *et al.*, 1983] and starlight [e.g., Esposito *et al.*, 1983] occultation data. This slab was modeled with monte carlo calculations as a target layer for interactions by high energy cosmic rays which can penetrate Saturn's magnetosphere and strike the rings at energies above 10-20 GeV/nucleon. The resultant interactions produce secondary radiation including neutrons, which then become parents via beta decay for the trapped high energy

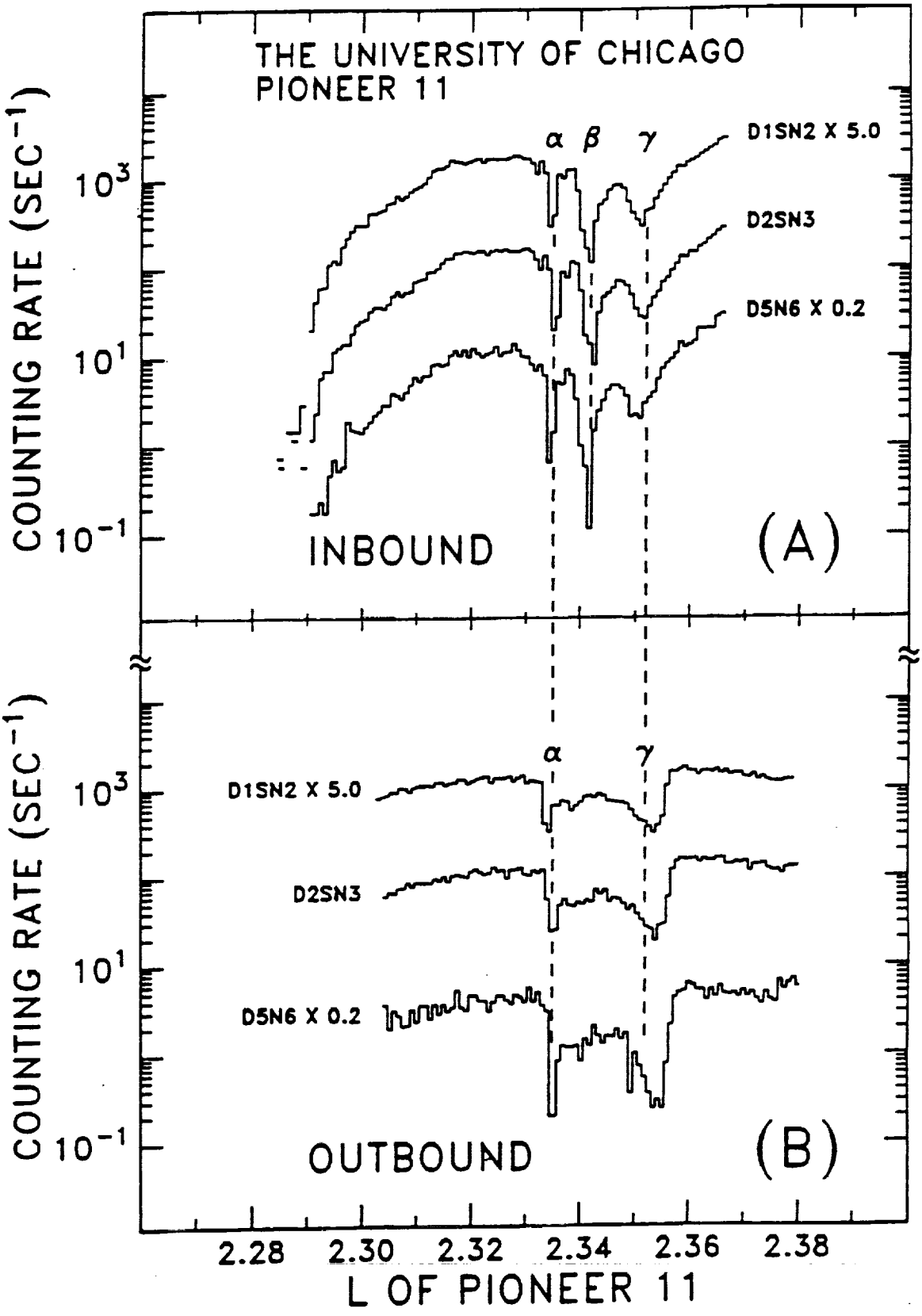

Figure 17: Inbound (A) and outbound (B) counting rates from Pioneer 11 [Simpson *et al.*, 1980a,b] for MeV electrons in the F-ring region where five microsignatures are evident. The flatter shapes of the outbound profiles are associated with the general drop in electron intensity inwards of 2.6 R_S. The "D5N6" profiles correspond nominally to "7-17 MeV electrons" from the University of Chicago's Main Telescope, while the other two profiles are accumulated from low-order coincidences of lower energy electrons in the front detectors of the same instrument.

protons. An important constraint on Cooper's original model was supplied by direct Pioneer 11 observations of secondary charged particles and gamma rays from these interactions in the rings [Chenette *et al.*, 1980; Cooper *et al.*, 1985; Van Allen and Randall, 1985]. These observations established that the observed secondary radiation intensities were consistent with results from the slab model and that the neutron emission could be accurately modeled.

Since free neutrons have average decay lifetimes of 10^3 seconds, only a very small fraction decay within the magnetosphere, so the injection rate of trapped, decay protons into the radiation belt regions is very small. We will use calculated profiles in Figure 18 of neutron-decay proton injection from Cooper's work to define the radial source profiles shown for different proton energies. The nearly exponential shapes of these profiles up to several hundred MeV allow simple parametric forms to be used for radial dependence of the source rates, which vary by factors of two or less between adjacent trapping regions. For narrow radial zones a constant source rate can be assumed.

Lossless Diffusion

Once injected, the trapped protons undergo radial diffusion at a rate determined by model fits to observations. Large trapping times ($\approx 10^0 - 10^2$ years) are required to build up significant fluxes at the levels observed. In the model the sweeping by satellites is treated by the definition of totally absorbing boundaries at the approximate positions of the satellites, where allowances are made in the fitting procedures for the finite gyroradii of the protons which increase the effective cross-sectional areas of the satellites for sweeping. Simple analytic forms for the solutions of radial transport equations with the CRAND source term, radial diffusion, and the satellite boundaries for each diffusion region are obtained in the limit that the proton profiles are time-independent. A principal limitation of the original model is that no attempt is made to include the obvious dust-related losses in the region of the G ring, the only modeled losses being those due to radial transport into regions of strong absorption from satellites and or rings, where the proton flux can be assumed to approach zero.

Figure 19 shows the results from Cooper [1983] for fits to University of Chicago profiles for high energy protons in the inner magnetosphere of Saturn. The energy-dependent response functions [Simpson *et al.* 1981; R. B. McKibben, unpublished data, 1982] of detectors giving the observed profiles have been folded into the model parameter fits. In general the diffusive gradients of the proton profiles are well-matched by the model curves in the vicinity of the satellite boundaries for a diffusion coefficient of the form $D_{LL} = D_0 L^n$, where $n = 9$ from the fit and $n = 10$ for diffusion driven by magnetic impulses from magnetospheric disturbances. In the region around the proton peak at 2.4 R_S the diffusive profile matches the observed reasonably well, while the fit is clearly not satisfactory in the G-ring region where dust losses have not been included in the model. Beyond 3.3 R_S the excess in the calculated rate relative to that measured indicates either that the source function requires correction or that E-ring losses should be included in the model. In principle, the profiles and relative intensities of the three major protons peaks can be totally explained in terms of the radial width of the lossless regions around the peaks and by the radial dependence of the source injection rate and of the diffusion coefficient. On the other hand, the observational and model-related uncertainties dictate that we estimate upper limits for potential losses having no obvious effect on the observed radial profiles.

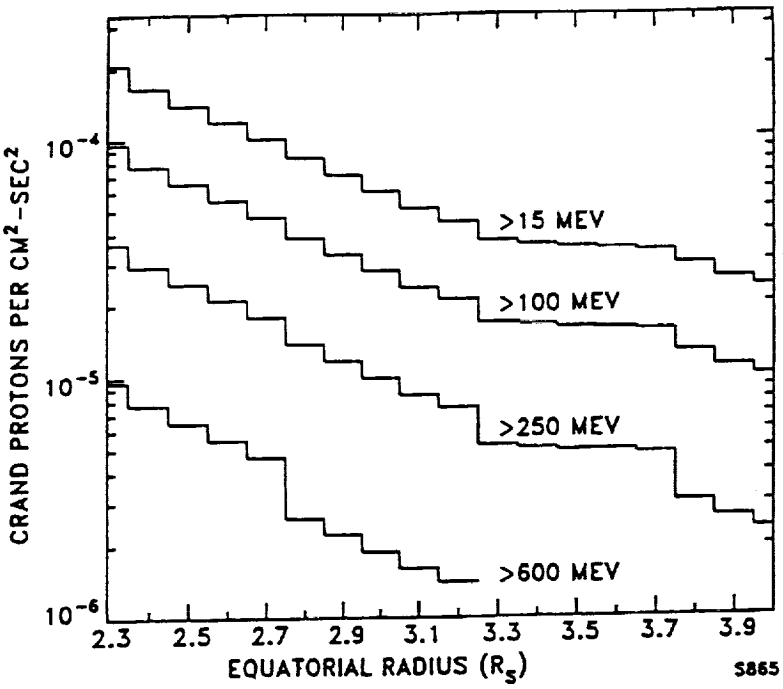

Figure 18: Radial profiles from Cooper [1983] for integral, omnidirectional injection rates of CRAND protons above selected energy thresholds.

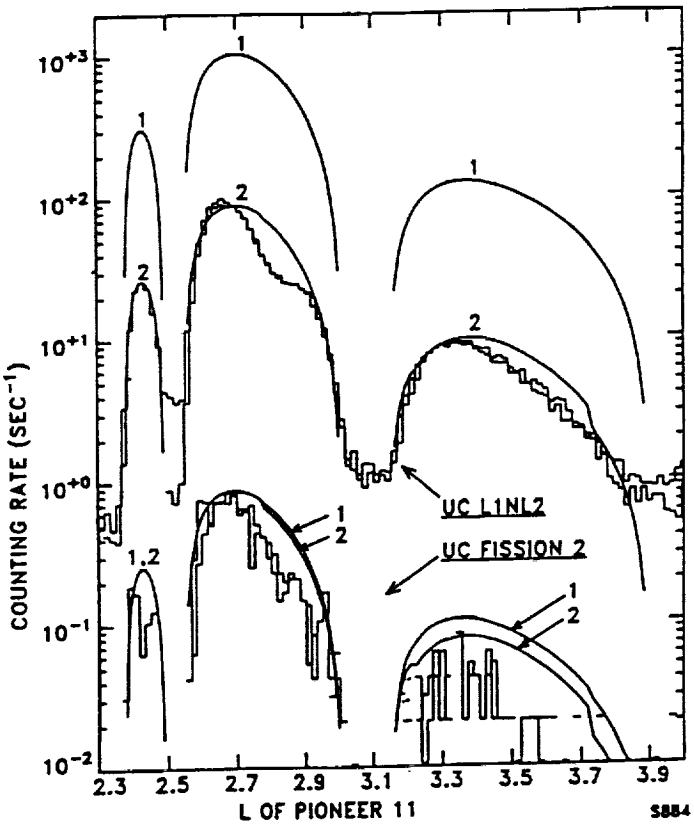

Figure 19: Best fits of the Cooper [1983] CRAND model to Pioneer 11 radial profiles from the University of Chicago for protons above 30 MeV. The fitted curves correspond to models including truncation of the calculated proton spectra and detector response functions below 15 MeV (1) and 250 MeV (2), where the latter was found to be most consistent with observed ratios of the two detector responses. The model curves are fitted to the observed absorption boundaries and the maximum proton intensities. Model fits to the three peaks are consistent with a diffusion coefficient $D_{LL} \approx 10^{-15} L^9 \; R_S{}^2/sec$ for protons $\geq 10^2$ MeV in the inner magnetosphere. The Cooper model did not include effects of proton absorption in the E ring. The divergence of the model curves from the data beyond is due either (1) to E ring absorption or (2) to radial changes in the source and injection geometry.

Radial Transport with CRAND and Losses

Using the CRAND model to set limits on dust abundances requires modification of the Cooper model to allow for distributed losses througout the diffusion region. The effects of satellite sweeping can still be retained in the boundary conditions as before. The most tractable solutions for the modified model arise when the losses are approximated by an average time scale for total loss which may be an analytic function of radial position and proton energy. Such solutions have previously been used [e.g., Hood, 1983, 1985] for lossy diffusion problems not including distributed sources. Work done in collaboration with Lon Hood has now generated the required solutions for distributed sources *and* losses. Development of these new solutions allows estimates to be made on upper limits for dust abundances, based on model fits to the observed radial profiles for high energy protons. Special cases of these solutions for the problems at hand are described in Hood's accompanying report. More detailed versions will be published later by Hood and myself.

The radial transport of charged particles in any stable, dipolar magnetic field is described by the following differential equation:

$$\frac{\partial \mathrm{f}}{\partial \mathrm{t}} + \mathrm{L}^2 \frac{\partial}{\partial \mathrm{L}} \left(\frac{\mathrm{D_{LL}}}{\mathrm{L}^2} \frac{\partial \mathrm{f}}{\partial \mathrm{L}} \right) + S - L = 0$$

This equation [e.g., Schulz and Lanzerotti, 1974] governs the time and spatial evolution of the phase space density function f(M, K, L) with respect to the three adiabatic invariants of charged particle motion: the magnetic moment M for gyromotion, the latitudinal bounce invariant K, and the radial parameter L defining the local field line. For simple calculations the usual procedure is to set K to zero in the limit of equatorially trapped particles, while allowing M and L to vary freely. Since the trapping times of CRAND protons are very long, the time dependent term $\partial \mathrm{f}/\partial \mathrm{t}$ is assumed to be negligible. The phase space space density is related to the differential particle flux j by $\mathrm{f} = \mathrm{j}/\mathrm{p}^2$, where p is the particle momentum on the local field line.

In the case of distributed injection by CRAND, there is little net acceleration, since protons diffuse both inwards and outwards from the intensity peaks, so we define an approximately constant momentum. In this case the phase space density is roughly proportional to the local integral flux at the level of the present analysis. It may also be more appropriate in such a case to use a one-dimensional transport equation of the form

$$\frac{\partial \mathrm{f}}{\partial \mathrm{t}} + \frac{\partial}{\partial \mathrm{L}} \left(\mathrm{D_{LL}} \frac{\partial \mathrm{f}}{\partial \mathrm{L}} \right) + S - L = 0$$

which can be easily solved in the simplest cases for constant values of $\mathrm{D_{LL}}$, S, and τ. These solutions are discussed in Hood's report.

The last three terms in the transport equation pertain to radial transport with diffusion coefficient $\mathrm{D_{LL}}$, the CRAND source injection rate S, and the loss rate L due to dust interactions and/or other processes. As for the phase space density, the source and loss terms are proportional (when multiplied by p^2) to the source and loss rates in flux units. We make further simplications by defining constant values for the source and loss terms, reasonably

The actual dust abundances could be quite close to the upper limit values and still have only marginally observable effects on the radial profiles for integral counting rates of CRAND protons, due to the competing losses from radial diffusion which steepen radial gradients in shoulder regions adjacent to intensity peaks. Hood's quantitative fits show that the "nominal" dust limits are a factor of three (i.e., an e-folding factor in loss time units) below the worst case values when the radial profiles are fitted with a one-dimensional, lossy diffusion model. On the other hand, these first order fits do not include effects of radial dependence in source and diffusion parameters, radial variations in proton energy and pitch angle distributions, or the effect of finite gyroradii (e.g., the gradient-anisotropy effect analysed by Northrop and Fillius [1985]). Thus, the worst cases values in Table 1 should be regarded as the more conservative estimates for impact risk assessments.

In comparison, the very substantial proton modulation by the G-ring (c.f., Figure 3) is associated with an estimated G-ring column density of $2x10^{-7}$ gm/cm^2, based on Hood's update of earlier modeling work done for the G ring by Van Allen [1983, 1987]. If the dust column density near the proton peak at 2.7 R_S is near the worst case value in Table 1, the higher proton intensity near the peak may actually lead to rates for proton interactions in dust which are within a factor of three of those in the G-ring region. Radial diffusion may also broaden the radial extent of regions effected by absorption in adjacent regions of stronger absorption. In this case, observable effects of absorption would be evident in more sensitive measurements over a broad radial range, even outside the principle absorption regions.

The Satellite Regions

Evaluated quantitatively, the microsignature observations yield very high estimates for column densities of co-orbiting material in the regions of observation. For the Mimas "ghost" microsignature we get a typical column density of order $1x10^{-2}$ gm/cm^2 for each clump of diameter 10^2 km by using parameters calculated by Chenette and Stone [1983]. Averaged over the width of the Mimas region (0.1 R_S) and the number of clumps ($\approx 3x10^3$) consistent with the observations, the "macrosignature" column density becomes $4x10^{-5}$ gm/cm^2. Although microsignatures in the Janus/Epimetheus and Tethys regions were clearly related to near encounters with known satellites (e.g., Van Allen, 1984), the observational statistics are such that we cannot rule out comparable amounts of co-orbiting material in those regions.

Another quantitative approach was first discussed by Schardt and McDonald [1983], who found that the measured fluxes and anisotropies for 63-160 MeV protons in the Mimas region could be consistent with absorption by Mimas alone. Their calculations employed the reasonably comparable CRAND sources from Cooper [1983] and Blake *et al.* [1983], theoretical derivations for proton sweeping by the satellite, and further assumed that proton lifetimes in this region were totally dominated by satellite losses and were unaffected by radial diffusion. Although they reported a four-fold coincidence measurement for the minimum proton intensity in the Mimas region, it may be assumed that there is some electron contamination in this measurement, the electron intensities being many orders of magnitude higher, so there remains a substantial margin for effects by other co-orbiting material. Our own analysis gives "worst case" lower limits of 10^{-6} to 10^{-5} gm/cm^2 for co-orbiting material absorbing CRAND protons at 2.35, 2.5, and 3.1 R_S and are consistent with the dust clump interpretation.

justifiable, since the source rate varies slowly with L, and we can only determine limits on the column density of a uniformly-thick dust layer in each diffusion region. The inner and outer edges of the strong absorption regions (i.e., orbits of principal satellites and the F ring) define zero-flux boundaries for the proton trapping regions (i.e,. proton gaps in our current parlance viz-a-viz Cassini aimpoints).

If one defines a characteristic time scale τ for dust losses, the loss term becomes $L = f/\tau$. In the limit of lossless diffusion, τ is set to infinity, while it assumes finite values for lossy diffusion. For proton losses in a vertically thin dust layer near the ring plane, the loss time scale is approximately

$$\tau = \frac{R_e T_B cos\alpha_0}{2\sigma}$$

where σ is the dust column density in units of gm/cm^2, R_e is the proton stopping range in the same units, T_B is the latitudinal bounce period in Saturn's dipole field [e.g., Thomsen and Van Allen, 1980], and the cosine factor ≈ 0.5 accounts for the inclined pathlength through the dust layer. We use stopping ranges in water ice of 7.7 gm/cm^2 for 100 MeV protons and 50 gm/cm^2 for 300 MeV protons.

4. Worst Case Limits for Dust Column Densities

High Intensity Regions

Our "worst case" limits for column densities of dust are determined simply by setting the integral source rate $\partial J_p/\partial t$ equal to the probabilistic loss rate J_p/τ, where J_p is the locally measured integral flux of protons at any given position in L, and then solving for σ in terms of the other, known parameters. This limit corresponds to the rather extreme assumption that the proton lifetimes are totally governed by losses in dust. Since it also corresponds to the critical values of σ at which the integral intensity extremes are either maximal ($S > L$) or minimal ($S < L$), the computed values of σ are upper limits near intensity peaks and lower limits near intensity minima. The computed limits, upper or lower, are shown in Table 1 for selected L positions. The proton fluxes (J_p) were computed from Pioneer 11 measurements of Fillius *et al.* [1980] for protons sampled near the magnetic equator (i.e., K $\approx$ 0) at energies above 80 MeV [c.f., Figure 3]. Since the form of the differential spectrum is not well-determined at 100-300 MeV, we show calculated limits for 100 MeV and 300 MeV protons, assuming that one or the other is characteristic of protons above the integral threshold energy.

The inverse proportionality between the calculated σ limits and the measured flux produces the lowest upper limit of 2-3x10^{-8} gm/cm^2 at the position of highest measured proton flux, L $\approx$ 2.65. The other two intensity peaks, located at 2.42 R_S and 3.3 R_S, give comparable upper limits of 1-2x10^{-7} gm/cm^2, an order of magnitude less than those at the most intense peak. If one assumes a uniform dust layer throughout the entire inner magnetosphere, except perhaps in the satellite regions where the calculated lower limits are 10^1 to 10^2 times higher, one might take the 2.65-R_S value of σ as the best-determined upper limit, simply because J_p is highest at that position. By this reasoning, the probable effects of dust in the two lower intensity peaks should therefore greatly reduced relative to the potentially marginal effect at the highest peak.

Table 1

CRAND Proton Limits for Dust Column Densities

L	σ (E=100) [gm/cm^2]	σ (E=300) [gm/cm^2]	
2.35	$\geq 3.5\text{x}10^{-5}$	$\geq 5.3\text{x}10^{-5}$	(F ring)
2.42	$\leq 9.6\text{x}10^{-8}$	$\leq 1.3\text{x}10^{-7}$	(Proton gap)
2.5	$\geq 2.8\text{x}10^{-5}$	$\geq 3.7\text{x}10^{-5}$	(Janus/Epimetheus)
2.65	$\leq 1.8\text{x}10^{-8}$	$\leq 2.7\text{x}10^{-8}$	(Proton gap)
2.80	$\geq 5.7\text{x}10^{-8}$	$\geq 7.5\text{x}10^{-8}$	(G ring)
3.1	$\geq 2.8\text{x}10^{-6}$	$\geq 3.4\text{x}10^{-6}$	(Mimas)
3.3	$\leq 1.6\text{x}10^{-7}$	$\leq 1.8\text{x}10^{-7}$	(Proton gap)
3.5	$\leq 3.5\text{x}10^{-7}$	$\leq 3.9\text{x}10^{-7}$	(E ring)
3.7	$\leq 1.3\text{x}10^{-6}$	$\leq 1.5\text{x}10^{-6}$	(E ring)

5. Justification for Relative Merits of Cassini Aimpoints

Proton Intensities

Our worst case limits for column density of dust are strongly correlated (inversely) to the local proton intensity. The only other well known parameter is the CRAND proton source which varies only by a factor of two between the two aimpoints. Since the measured proton intensity is a factor of ten higher at 2.7 R_S than at 3.2 R_S, I would feel safer going in at the inner point, just because the higher proton intensity there is a better probe of the dust density. The same argument applies to a comparison between 2.7 R_S and the innermost "proton gap" centered on 2.42 R_S, the first being preferable to the second.

In general, the relative intensity levels in all three gaps are consistent with our expectations for effects of CRAND and lossless diffusion as demonstrated in Figure 19. The increase in the radial diffusion rate by a factor of five (for $D_{LL} \propto L^9$) at 3.2 R_S gives a relatively stronger diffusive loss effect which mostly accounts for the lower intensity. An additional factor of two from radial dependence of the source rate further accounts for the order of magnitude difference in intensity between the peaks at 2.7 and 3.2 R_S. Similarly, the lower diffusion rate, and the slightly higher source rate, in the 2.42-R_S gap compensate for the relatively smaller radial width of this gap and account for the observed intensity.

About all the integral intensity profiles can tell us is the upper limit on a uniformly thick dust layer, except perhaps in the satellite regions, throughout the entire inner magnetosphere. The best constraint on this is determined at 2.7 R_S where $\sigma \leq$2-3x10^{-8} gm/cm^2 for the 100-300 MeV protons dominating the measured integral intensities. If the dust effect there is

marginal (i.e., within a factor of three of the worst case limit) , there should be less observable effects in integral intensity profiles in the other proton gaps. For these the lower intensities give correspondingly lower proton impact rates on dust relative to loss rates from radial transport into the strong absorption regions of the satellite orbits.

Proton Energy Spectra

Although the CRAND model fits to integral intensity profiles are consistent with lossless (i.e., no dust) diffusion at 2.7 R_S and elsewhere, higher sensitivity might be achieved by looking at protons below 100 MeV where ionization energy losses are more significant. Indeed, some data from Voyager [Armstrong and Krimigis, 1982] indicate dropoff towards MeV energies in spectra measured near 2.73 R_S and near 3.4 R_S. Other spectra from Schardt and McDonald [1983] do not show this dropoff, but probably have significant electron contamination at the lower energies (27-63 MeV as compared to 63-160 MeV). From these data I infer a significant dust absorption effect for the lower energy protons. Since the proton energy loss range increases by an order of magnitude from the lower energies to 300 MeV, the dust effect might be significant for the lower energies while still being very marginal at the higher energies which dominate the integral counting rates used for the radial profile fits. Thus I doubt that the real dust column density is much less than an order of magnitude below the worst case limit for 2.7 R_S, when the spectral information is considered. Furthermore, the potential evidence for secondary electron production in the proton gaps argues for some finite, but yet to be determined amount of diffuse material. On the other hand, there may other explanations for the proton spectra and high energy electron results, so these cannot be considered as very definitive at this point in terms of providing information on dust limits.

Proton Anisotropies

The anisotropy peak at 3.2-3.4 R_S in the Schardt and McDonald [1983] data certainly suggests that this region is relatively clear of absorbers as compared to the G-ring and the Mimas region. Since one is still apparently within the influence of the G-ring via diffusion at Voyager 2's innermost L-shell of 2.73 R_S, the Voyager 2 measurement there may not tell us anything about the actual anisotropy near the peak intensity level at 2.65 R_S. However, Van Allen *et al.* [1980b] did note that roll modulation in their Pioneer 11 counting rates was consistent with a high degree of anisotropy ($n \approx 4$), but they did not specify the radial dependence. Close examination of Figure 4 in their Science paper [Van Allen *et al.*, 1980a] shows no significant variation in the roll modulation of the rates for >80-MeV protons in the region at 2.6-2.8 R_S, so it is unclear whether the anisotropy increases from a low level at 2.8 R_S in the Voyager measurement (c.f., Figure 11) to the high level estimated from the Pioneer data further inwards. One might also note that the roll modulation in the Pioneer 11 data is just as large at 2.42 R_S as in the 2.65 R_S gap, as determined from the proton profiles published by Van Allen *et al.* and by Fillius *et al.* [1980], where data from the latter can be seen in our Figure 2.

Thus the available anisotropy data do not address the relative merits of aimpoints in the three proton gaps, but the Voyager data in Figure 11 do indicate more definitively that 3.2 R_S is in a good region from the standpoint of high anisotropy. The higher proton intensity at 2.65 R_S suggests that one might find a larger anisotropy there, but the published Pioneer 11 show no discernable difference from that found elsewhere, including at 2.8 R_S where Figure 11 shows a low anisotropy level. Additional input from the Pioneer 11 investigators (e.g.,

Van Allen *et al.*, Fillius *et al.*) would be desirable to allow study of the available, unpublished anisotropy data in the inner regions covered by Pioneer 11.

The general decline in anisotropy beyond 3.4 R_S is conceivably related to dust absorption and might be correlated to the radial variation of the E-ring dust density which peaks near Enceladus, but existing models are not adequate to decide whether a CRAND source effect is the more likely explanation. This needs more work and might also reveal something interesting about large particle distributions in the main rings which emit the parent neutrons for CRAND. Until one understands this better, I would be inclined to move the most critical (e.g., SOI) aimpoints as far away from Enceladus's orbit as possible and would again choose 2.7 over 3.2 R_S. The available anisotropy data do not rule out an aimpoint even at 2.42 R_S.

Potential Pathological Problems

Are the sub-MeV ion and electron measurements inside 5 R_S relevant for constraints on E-ring densities? Considering the not-so-pathological scenario that I have conceived for the Voyager 2 LECP response to MeV electrons in this region, I will personally have no confidence at all in these data until laboratory experiments (easily done) establish that internal backscattering of MeV electrons cannot explain the observations. I strongly believe that Van Allen's early reservations about instrument backgrounds from the electrons, having a drift resonance peak in differential spectra near 1.0-1.2 MeV (i.e., not sufficient to penetrate the LECP sun shield used to check for background response), require much further scrutiny with laboratory and theoretical investigations before final decisions are made about E-ring hazards.

The microsignature observations may have similar problems, as Van Allen *et al.*'s [1980c] analysis of electron background was specifically designed to address. The LECP pathology would affect interpretation of the Carbary *et al.* [1983] data for microsignatures in low energy electrons and ions, which nominally verify the presence of dust clumps in the Mimas and Enceladus regions. The CRS data of Chenette and Stone [1983] require further analysis in light of recent calibration results indicating more complicated energy response some of the detectors used for their analysis in the Mimas region. The possibility of electron contamination in the pulse height data of Simpson *et al.* [1980b, 1981] also requires further study for the Mimas region. Accepted otherwise at face value, the published microsignature observations indicate potentially large abundances of co-orbiting material and correspondingly grave impact hazards for ring plane crossings by Cassini in the vicinity of the principal satellite orbits.

References

Blake, J. B., H. Hilton, and S. H. Margolis, On the injection of cosmic ray secondaries into the inner Saturnian magnetosphere, 1. Protons from the CRAND process, *J. Geophys. Res.*, *88*, 803, 1983.

Carbary, J. F., S. M. Krimigis, and W.-H. Ip, Energetic particle signatures of Saturn's satellites, *J. Geophys. Res.*, *88*, 8947, 1983.

Chenette, D. L., J. F. Cooper, J. H. Eraker, K. R. Pyle, and J. A. Simpson, High-energy trapped radiation penetrating the rings of Saturn, *J. Geophys. Res.*, *85*, 5785, 1980.

Chenette, D. L., and E. C. Stone, The Mimas ghost revisited: an analysis of the electron flux and electron microsignatures observed in the vicinity of Mimas at Saturn, *J. Geophys.*

Res., 88, 8755, 1983.

Cooper, J. F., Nuclear cascades in Saturn's rings: Cosmic ray albedo neutron decay and origins of trapped protons in the inner magnetosphere, *J. Geophys. Res., 88*, 3945, 1983.

Cooper. J. F., J. H. Eraker, and J. A. Simpson, The secondary radiation under Saturn's A-B-C rings produced by cosmic ray interactions, *J. Geophys. Res., 90*, 3415, 1985.

Cuzzi, J. N., and J. A. Burns, Charged particle depletion surrounding Saturn's F ring: Evidence for a moonlet belt?, *Icarus, 74*, 284, 1988.

Esposito, L. W., J. M. Cuzzi, D. R. Evans, J. B. Holberg, E. A. Marouf, and C. C. Porco, Saturn's rings: structure dynamics and particle properties, in *Saturn*, chap. 12, University of Arizona Press, Tucson, 1983.

Fillius, W., W.-H. Ip, and C. E. McIlwain, Trapped radiation belts at Saturn: first look, *Science, 207*, 425, 1980.

Fillius, W., J. F. Cooper, and R. B. McKibben, Review of Pioneer 11 data for high energy trapped radiation in Saturn's magnetosphere, *Trans. Amer. Geophys. Union (EOS), 69*, 1398, 1988.

Fillius, W., and C. M. McIlwain, Very energetic protons in Saturn's radiation belt, *J. Geophys. Res., 85*, 5803, 1980.

Hood, L. L., Radial diffusion in Saturn's radiation belts: a modeling analysis assuming satellite and ring E absorption, *J. Geophys. Res., 88*, 808, 1983.

Hood, L. L., Radial diffusion of low-energy ions in Saturn's radiation belts: a combined analysis of phase space density and satellite microsignature data, *J. Geophys. Res., 90*, 6295, 1985.

Konradi, A., Effect of the orbital debris environment on the high-energy Van Allen proton belt, *Science, 242*, 1284, 1988.

Krimigis, S. M., and T. P. Armstrong, Two-component proton spectra in the inner Saturnian magnetosphere, *Geophys. Res. Lett., 9*, 1143, 1982.

Krimigis, S. M., J. F. Carbary, E. P. Keath, T. P. Armstrong, L. J. Lanzerotti, and G. Gloeckler, General characteristics of hot plasma and energetic particles in the Saturnian magnetosphere: results from the Voyager 2 spacecraft, *J. Geophys. Res., 88*, 8871, 1983.

Marouf, E. A., G. L. Tyler, H. A. Zebeker, R. A. Simpson, and V. R. Eshleman, Particle-size distributions in Saturn's rings from Voyager 1 radio occultations, *Icarus, 54*, 189, 1983.

McDonald, F. B., A. W. Schardt, and J. H. Trainor, If you've seen one magnetosphere, you haven't seen them all: energetic charged particle observations in the Saturn magnetosphere, *J. Geophys. Res., 85*, 5813, 1980.

Nicholson, P., "Cassini Science at SOI: Recommended Options," Report to Joint ESA-NASA Cassini Science Working Group, Toulouse, France, April, 1989.

Northrop, T. G., and W. Fillius, Electrons and cosmic ray produced protons in Saturn's inner magnetosphere, *J. Geophys. Res., 90*, 12085, 1985.

Opp, A. G., Scientific results from the Pioneer Saturn encounter: Summary, *Science, 207*, 401, 1980.

Scarf, F. F., D. A. Gurnett, W. S. Kurth, and R. L. Poynter, Voyager-2 plasma wave observations at Saturn, *Science, 215*, 587, 1982.

Scarf, F. F., D. A. Gurnett, W. S. Kurth, and R. L. Poynter, Voyager plasma wave measurements at Saturn, *J. Geophys. Res., 88*, 8971, 1983.

Schardt, A. W., The magnetosphere of Saturn, *Rev. of Geophys. and Sp. Sci., 21*, 390, 1983.

Schardt, A. W., and F. B. McDonald, The flux and source of energetic protons in Saturn's inner magnetosphere, *J. Geophys. Res., 88*, 8923, 1983.

Schulz, M., and L. J. Lanzerotti, *Particle Diffusion in the Radiation Belts*, Springer-Verlag, New York, 1974.

Simpson, J. A., T. S. Bastian, D. L. Chenette, G. A. Lentz, R. B. McKibben, K. R. Pyle, and A. J. Tuzzolino, Saturnian trapped radiation and its absorption by satellites and rings: the first results from Pioneer-11 *Science, 207*, 411, 1980a.

Simpson, J. A., T. S. Bastian, D. L. Chenette, R. B. McKibben, and K. R. Pyle, The trapped radiations of Saturn and their absorption by satellites and rings, J. Geophys. Res., 85, 5731, 1980b.

Simpson, J. A., T. S. Bastian, D. L. Chenette, R. B. McKibben, and K. R. Pyle, Interim report on the re-examination of the University of Chicago measurements of low-energy proton fluxes in the region 2.3 ¡ L ¡ 4.0 at Saturn, *EFI Rep. 81-34*, Univ. of Chicago, Chicago, 1981.

Stetson, D., Overview of Cassini mission profile, invited talk presented at workshop "Scientific Goals for Cassini: Saturn's Rings," Pasadena, California, June 27, 1988.

Stone, E. C., and E. D. Miner, Voyager 1 encounter with the saturnian system, *Science, 212*, 159, 1981.

Stone, E. C., and E. D. Miner, Voyager 2 encounter with the saturnian system, *Science, 215*, 499, 1982.

Trainor, J. H., F. B. McDonald, and A. W. Schardt, Observations of energetic ions and electrons in Saturn's magnetosphere, *Science, 207*, 421, 1980.

Tyler, G. L., E. A. Marouf, R. A. Simpson, H. A. Zebker, and V. R. Eshleman, The microwave opacity of Saturn's rings at wavelengths of 3.6 and 13 cm from Voyager 1 radio occultations, *Icarus, 54*, 160, 1982.

Van Allen, J. A., Absorption of energetic protons by Saturn's ring G, *J. Geophys. Res., 88*, 6911, 1983.

Van Allen, J. A., Energetic particles in the inner magnetosphere of Saturn, in *Saturn*, edited by T. Gehrels and M. S. Matthews, University of Arizona Press, Tucson, 1984.

Van Allen, J. A., An upper limit on the sizes of sheparding satellites at Saturn's ring G, *J. Geophys. Res., 92*, 1153, 1987.

Van Allen, J. A., M. F. Thomsen, B. A. Randall, R. L. Rairden, and C. L. Grosskreutz, Saturn's magnetosphere, rings, and inner satellites, *Science, 207*, 415, 1980a.

Van Allen, J. A., B. A. Randall, and M. F. Thomsen, Sources and sinks of energetic electrons and protons in Saturn's magnetosphere, *J. Geophys. Res., 85*, 5679, 1980b.

Van Allen, J. A., M. F. Thomsen, and B. A. Randall, The energetic charged particle signature of Mimas, *J. Geophys. Res., 85*, 5709, 1980c.

Van Allen, J. A., and B. A. Randall, Interplanetary cosmic ray intensity: 1972-1984 and out to 32 A.U., *J. Geophys. Res., 90*, 1399, 1985.

Vogt, R. E., D. L. Chenette, A. C. Cummings, T. L. Garrard, E. C. Stone, A. W. Schardt, J. H. Trainor, N. Lal, and F. B. McDonald, Energetic charged particles in Saturn's magnetosphere: Voyager 2 results, Science, 215, 577, 1982.